On the real-time evolution of pseudo-entropy in 2d CFTs

Wu-zhong Guo[b,1], Song He[a,c,2], Yu-Xuan Zhang[a,3]

[a] *Center for Theoretical Physics and College of Physics, Jilin University,*
Changchun 130012, People's Republic of China
[b] *School of Physics, Huazhong University of Science and Technology*
Luoyu Road 1037, Wuhan, Hubei 430074, China
[c] *Max Planck Institute for Gravitational Physics (Albert Einstein Institute),*
Am Mühlenberg 1, 14476 Golm, Germany

Abstract

In this work, we study the real-time evolution of pseudo-(Rényi) entropy, a generalization of entanglement entropy, in two-dimensional conformal field theories (CFTs). We focus on states obtained by acting primary operators located at different space points or their linear combinations on the vacuum. We show the similarities and differences between the pseudo-(Rényi) entropy and entanglement entropy. For excitation by a single primary operator, we analyze the behaviors of the 2nd pseudo-Rényi entropy in various limits and find some symmetries associated with the subsystem and the positions of the inserted operators. For excitation by linear combinations, the late time limit of the nth pseudo-Rényi entropy shows a simple form related to the coefficients of the combinations and Rényi entropy of the operators, which can be derived by using the Schmidt decomposition. Further, we find two kinds of particular spatial configurations of insertion operators in one of which the pseudo-(Rényi) entropy remains real throughout the time evolution.

---

[1]wuzhong@hust.edu.cn
[2]hesong@jlu.edu.cn; corresponding author
[3]yuxuanz18@mails.jlu.edu.cn; corresponding author

Contents

1   Introduction

Entanglement entropy, a physical observable stemming from quantum information, has now pervaded many branches of theoretical physics such as quantum many-body physics [1–3], high energy physics [4–8], gravitational physics [9–13], and so on. It is worth mentioning that recently, its quantum corrected holographic version [9,10], a.k.a. quantum extremal surface [14], in the AdS/CFT correspondence [15–17] has played a crucial role in solving problems such as black hole information loss [18, 19], providing a reliable way to further understand quantum gravity.

Also recently, a new quantity associated with a bulk minimal area surface, called pseudo-entropy, has been introduced in [20] under the framework of AdS/CFT correspondence. Given a total system $\mathcal{S}$, one can define the pseudo-entropy associated with a subsystem A in terms of

the corresponding pseudo-Rényi entropy

$$S_A^{(n)} \equiv \frac{1}{1-n} \log \mathrm{Tr}\big[(\mathcal{T}_A^{1|2})^n\big], \quad (n > 1, \ n \in \mathbb{Z}), \tag{1}$$

where the matrix $\mathcal{T}_A^{1|2}$ involved two nonorthogonal quantum states $|\psi_1\rangle, |\psi_2\rangle \in \mathcal{H}_\mathcal{S}$, named reduced transition matrix, is the partial trace of the transition matrix $\mathcal{T}^{1|2}$,[4]

$$\mathcal{T}^{1|2} \equiv \frac{|\psi_1\rangle\langle\psi_2|}{\langle\psi_2|\psi_1\rangle}, \quad \mathcal{T}_A^{1|2} \equiv \mathrm{Tr}_{A^c}\big[\mathcal{T}^{1|2}\big]. \tag{2}$$

The pseudo-entropy of subsystem A

$$S_A \equiv -\mathrm{Tr}\big[\mathcal{T}_A^{1|2} \log \mathcal{T}_A^{1|2}\big] \tag{3}$$

is obtained by taking the limit of $n \to 1$ for $S_A^{(n)}$. The reduced transition matrix is not Hermitian in general; hence the pseudo-entropy usually takes complex values. However, the results in the qubit system suggest that the real part of pseudo-entropy can be used to characterize the number of distillable Bell pairs averaged over the histories between the initial and final state [20]. More intriguingly, it was recently found in [21] that the real-time evolution of the real part of pseudo entropy follows the Page curve [22] under some field-theoretic settings based on the black hole final state proposal [23]. [5] Hence pseudo-entropy, like entanglement entropy, can reflect certain underlying correlation structures. Refer to [25–31] for other related developments of pseudo-entropy.

The main purpose of this paper is to study the real-time evolution of the real part of pseudo-entropy for locally excited state generated by a single primary operator or linear combination of a bunch of them in various 2d CFTs. Unlike the case in [21], our investigation can be regarded as a pseudo-entropy extension of the real-time evolution of the entanglement entropy after such local operator excitations [32]. In recent years, the time evolution of entanglement entropy for locally excited states has been widely studied, including rational CFTs [33–35], irrational CFTs [36], large-c CFTs [37, 38], boundary CFTs [39], warped CFTs [40], CFTs at finite temperature [41], multiple local excitations [42], and holographic duals of the local excitations [43–46]. In 2d rational CFTs (RCFTs), it was found that the variation of nth Rényi entropy for locally primary excited states saturates to a constant equal to the logarithm of the quantum dimension of the local operator's conformal family [33–35]. Such saturation get well interpreted in the picture of propagation of quasiparticles pairs [32, 47]. On the other hand, it was found in large-c CFTs [37, 38] that a characteristic feature called scrambling of entanglement would scramble the information of non-perturbative constants like quantum dimensions and lead to a logarithmically diverged Rényi entropy [37, 48].

---

[4]A^c refer to the complement of A and we have assumed that the Hilbert space of total system $\mathcal{H}_\mathcal{S}$ can be divided into $\mathcal{H}_A \bigotimes \mathcal{H}_{A^c}$.

[5]More recently, the authors of [24] reproduce the Page curve in another purely field-theoretic way called moving mirror.

Since pseudo-entropy is a straightforward generalized concept of entanglement entropy, we shall study the time evolution behavior of pseudo-entropy for locally excited states in various 2d CFTs. We set up various situations to calculate the pseudo-entropy of locally excited states in 2d rational CFTs and large-c CFTs and to explore universal properties of pseudo entropy of locally excited states.

This paper is organized as follows. Section 2 outlines the standard replica method to compute the nth pseudo-Rényi entropy for locally excited states. In Section 3 we mainly focus on the case of $n = 2$. We first study the limiting behaviors of real-time evolution of 2nd pseudo-Rényi entropy in rational CFTs and large-c CFTs. We then numerically analyze the full-time evolutions of 2nd pseudo-Rényi entropy in some specific interacting theories. In Section 4, we extend the above analysis to the nth pseudo-Rényi entropy. We end in Section 5 with conclusions and prospects. Some useful formulae and calculation details are presented in the appendices.

2   General calculations of pseudo-Rényi entropy

2.1   Setup for local excitations and $S_A^{(n)}$ from replica method

In this section, we review the replica calculation for the pseudo-Rényi entropy [20], which is almost same with that for the ordinary Rényi entropy [6]. Consider a 2d CFT dwells on a plane Σ_1 with coordinates $\{\tau, \ x\}$ ($\mathrm{d}s^2 = \mathrm{d}\tau^2 + \mathrm{d}x^2$). We are primarily interested in the cases that $|\psi_1\rangle$, $|\psi_2\rangle$ are states defined by acting various operators on the ground state $|\Omega\rangle$,

$$|\psi_j\rangle = \frac{1}{\sqrt{\mathcal{N}_j}} \mathcal{O}_{j,1}(-\tau_{j,1}, x_{j,1}) \mathcal{O}_{j,2}(-\tau_{j,2}, x_{j,2})...\mathcal{O}_{j,n_j}(-\tau_{j,n_j}, x_{j,n_j})|\Omega\rangle, \tag{4}$$

$$(\tau_{j,i+1} \geq \tau_{j,i} > 0, \ i = 1, 2, ..., n_j - 1; \ j = 1, 2),$$

where $\mathcal{N}_j$ is normalization factor and $\mathcal{O}_{j,i}(-\tau_{j,i}, x_{j,i}) \equiv e^{-H\tau_{j,i}} \mathcal{O}_{j,i}(x_{j,i}) e^{H\tau_{j,i}}$ is operator located at $(\tau = -\tau_{j,i}, x = x_{j,i})$. We can write down the corresponding transition matrix (2) in terms of the path integral language as follows

$$\mathcal{T}^{1|2} = \frac{\mathcal{O}_{1,1}(-\tau_{1,1}, x_{1,1})...\mathcal{O}_{1,n_1}(-\tau_{1,n_1}, x_{1,n_1})|\Omega\rangle\langle\Omega|\mathcal{O}_{2,n_2}^\dagger(\tau_{2,n_2}, x_{2,n_2})...\mathcal{O}_{2,1}^\dagger(\tau_{2,1}, x_{2,1})}{\langle\Omega|\mathcal{O}_{2,n_2}^\dagger(\tau_{2,n_2}, x_{2,n_2})...\mathcal{O}_{2,1}^\dagger(\tau_{2,1}, x_{2,1})\mathcal{O}_{1,1}(-\tau_{1,1}, x_{1,1})...\mathcal{O}_{1,n_1}(-\tau_{1,n_1}, x_{1,n_1})|\Omega\rangle}$$

$$\tag{5}$$

Here the dashed lines represent the free boundaries, and the stars denote the insertion points of the operators. The reduced transition matrix of the subsystem A is obtained by "stitching

up" the upper and lower edges of A^c

$$\mathcal{T}_A^{1|2} = \mathrm{Tr}_{A^c}\left[\mathcal{T}^{1|2}\right] = \left(\;\boxed{}\;\right)^{-1} \times \;\boxed{}\;. \tag{6}$$

Substituting (6) into (1), the path integral representation of $S_A^{(n)}$ is given by

$$S_A^{(n)} = \frac{1}{1-n}\log\left[\left(\;\boxed{}\;\right)^{-n} \times \underbrace{\boxed{}}_{\Sigma_n}\right]$$

$$= S_{A;vac}^{(n)} + \frac{1}{1-n}\left(\log\left\langle(\mathcal{O}_{2,n_2}^{\dagger(n)}...\mathcal{O}_{1,n_1}^{(n)})...(\mathcal{O}_{2,n_2}^{\dagger(1)}...\mathcal{O}_{1,n_1}^{(1)})\right\rangle_{\Sigma_n} - n\log\left\langle\mathcal{O}_{2,n_2}^{\dagger}...\mathcal{O}_{1,n_1}\right\rangle_{\Sigma_1}\right). \tag{7}$$

In the above, $S_{A;vac}^{(n)}$ stands for the nth Rényi entropy of A when the total system is in vacuum state, and Σ_n is a n-sheeted Riemann surface constructed by gluing n sheets Σ_1 together at subsystem A. The subscript of $\mathcal{O}^{(k)}$ denotes that the operator $\mathcal{O}$ is living on the kth sheet of Σ_n. Since $S_{A;vac}^{(n)}$ does not carry any information about excitations, we shall focus on the excess $\Delta S_A^{(n)} \equiv S_A^{(n)} - S_{A;vac}^{(n)}$ hereafter.

2.2   The excess of second pseudo-Rényi entropy $\Delta S_A^{(2)}$

Let us first concentrate on the simplest case that $n_1 = n_2 = 1$, $n = 2$. In the meantime, we are mainly interested in the case where two inserted operators are the same. Now (4) can be reduced to

$$|\psi_j\rangle = \frac{1}{\sqrt{\mathcal{N}_j}}\mathcal{O}(-\tau_j, x_j)|\Omega\rangle, \quad (j = 1, 2), \tag{8}$$

and the corresponding excess of pseudo-Rényi entropy is given by

$$\Delta S_A^{(2)} = -\log\frac{\left\langle\mathcal{O}^{\dagger(2)}(\tau_2, x_2)\mathcal{O}^{(2)}(-\tau_1, x_1)\mathcal{O}^{\dagger(1)}(\tau_2, x_2)\mathcal{O}^{(1)}(-\tau_1, x_1)\right\rangle_{\Sigma_2}}{\left\langle\mathcal{O}^{\dagger}(\tau_2, x_2)\mathcal{O}(-\tau_1, x_1)\right\rangle_{\Sigma_1}^2}. \tag{9}$$

The above expression is reduced to two- and four-point functions that we know for precisely solvable CFTs. It coincides with the excess of the second Rényi entropy when the insertion points are symmetric about the x-axis, i.e., $\tau_1 = \tau_2$ and $x_1 = x_2$. Owing to the conformal

symmetry, when $\mathcal{O}$ is a primary operator with chiral and antichiral conformal dimension $\Delta_{\mathcal{O}}$, the two-point and four-point function of $\mathcal{O}$ on Σ_1 are given by[6]

$$\langle \mathcal{O}^\dagger(z_2, \bar{z}_2) \mathcal{O}(z_1, \bar{z}_1) \rangle_{\Sigma_1} = \frac{c_{12}}{|z_{12}|^{4\Delta_{\mathcal{O}}}}, \tag{10}$$

$$\langle \mathcal{O}^\dagger(z_4, \bar{z}_4) \mathcal{O}(z_3, \bar{z}_3) \mathcal{O}^\dagger(z_2, \bar{z}_2) \mathcal{O}(z_1, \bar{z}_1) \rangle_{\Sigma_1} = |z_{13} z_{24}|^{-4\Delta_{\mathcal{O}}} G(\eta, \bar{\eta}), \tag{11}$$

respectively, where $(\eta, \bar{\eta}) \equiv \left(z_{12} z_{34}/(z_{13} z_{24}), \ \bar{z}_{12} \bar{z}_{34}/(\bar{z}_{13} \bar{z}_{24}) \right)$ are cross ratios and c_{12} is normalization factor. Since we can apply the conformal transformation

$$z = \left(\frac{w}{w - L} \right)^{1/n}, \quad (A = [0, L]), \tag{12}$$

$$z = w^{1/n}, \quad\quad\quad (A = [0, +\infty)), \tag{13}$$

to map Σ_n to Σ_1, we obtain the four-point function on Σ_2 by applying the above conformal maps with $n = 2$

$$\langle \mathcal{O}^\dagger(w_4, \bar{w}_4) \mathcal{O}(w_3, \bar{w}_3) \mathcal{O}^\dagger(w_2, \bar{w}_2) \mathcal{O}(w_1, \bar{w}_1) \rangle_{\Sigma_2} = \begin{cases} \left| \frac{16 L^2 z_1^2 z_2^2}{(z_1^2 - 1)^2 (z_2^2 - 1)^2} \right|^{-4\Delta_{\mathcal{O}}} G(\eta, \bar{\eta}) & (A = [0, L]), \\[2ex] \left| 16 z_1^2 z_2^2 \right|^{-4\Delta_{\mathcal{O}}} G(\eta, \bar{\eta}) & (A = [0, +\infty)), \end{cases} \tag{14}$$

where we have set

$$(w_3, \bar{w}_3)_{\text{sheet 2}} = (w_1, \bar{w}_1)_{\text{sheet 1}} = (x_1 - i\tau_1, x_1 + i\tau_1),$$

$$(w_4, \bar{w}_4)_{\text{sheet 2}} = (w_2, \bar{w}_2)_{\text{sheet 1}} = (x_2 + i\tau_2, x_2 - i\tau_2), \tag{15}$$

as shown in figure 1. Combining (14) with (10), the excess of the second pseudo-Rényi entropy
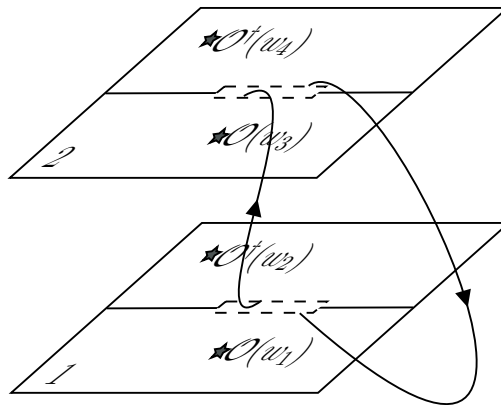
Figure 1: The 2-sheeted space Σ_2. The dashed box represents the subsystem A.

(9) is expressed as a function which depends only on η and $\bar{\eta}$

$$\Delta S_A^{(2)} = \log \frac{c_{12}^2}{|\eta(1 - \eta)|^{4\Delta_{\mathcal{O}}} \cdot G(\eta, \bar{\eta})}. \tag{16}$$

---

[6] $\{z, \bar{z}\} := \{x + i\tau, x - i\tau\}$ are complex coordinates on Σ_1, likewise for complex coordinates $\{w, \bar{w}\}$ on Σ_n. $z_{ij} \equiv z_i - z_j$.

3 Real-time evolution of $\mathrm{Re}[\Delta S_A^{(2)}]$

The real-time evolution of the pseudo-Rényi entropy for locally excited states can be regarded as a generalization of that of the Rényi entropy for locally excited states [32–37, 39, 41, 49]. In rational CFTs, it is known that the excess of the Rényi entropy saturates to a constant equal to the logarithm of the quantum dimension of the inserted primary operator [32, 33]. A similar result for pseudo-Rényi entropy is found in free CFT in [20]. However, [20] only consider the real-time evolution of pseudo-Rényi entropy with different insertion time and the same insertion spatial coordinates. Richer evolutionary structures seem to lie in another insertion configuration of operators—two operators with different spatial coordinates and the same insertion time. In this section, we mainly explore this insertion configuration and give a general argument in the light of [33].

3.1 $\Delta S_A^{(2)}$ for two primary operators with different spatial coordinates

In the following, we explore the case where the time coordinates of the two inserted operators are the same, but the spatial coordinates are different. That is, we are considering the following real-time dependent transition matrix

$$\mathcal{T}^{1|2}(t) \equiv \frac{e^{-iHt}e^{-\epsilon H}\mathcal{O}(x_1)|\Omega\rangle\langle\Omega|\mathcal{O}^\dagger(x_2)e^{-\epsilon H}e^{iHt}}{\langle\Omega|\mathcal{O}^\dagger(x_2)e^{-2\epsilon H}\mathcal{O}(x_1)|\Omega\rangle}, \quad \mathcal{T}_A^{1|2}(t) \equiv \mathrm{Tr}_{A^c}[\mathcal{T}^{1|2}(t)]. \tag{17}$$

It amounts to perform the following analytic continuation for τ_1, τ_2 in (8):

$$\tau_1 = \epsilon + it, \quad \tau_2 = \epsilon - it, \tag{18}$$

wherein $\epsilon > 0$ is an infinitesimally small regularization parameter to suppress the high energy modes [47].

3.1.1 Early time, middle time, and late time behaviors

Let us first study some limiting behaviors of the pseudo-Rényi entropy to obtain some generic conclusions. The procedure is similar to that of entanglement entropy [33, 37]. For the subsystem A of infinite length, we are mainly interested in the early time and late time limits of pseudo-Rényi entropy, while for the subsystem A of finite length, we are also interested in the middle time limit.[7]

The subsystem $A = [0, \infty)$: Consider the case of $A = [0, \infty)$, in which we are mainly interested in the early ($t \to 0$) and late ($t \to +\infty$) time limits. According to the expression of

---

[7]Based on the result of entanglement entropy in finite scales [33], the middle time may be defined as the interval $[u, v]$, where $u = \min\left[|x_1|, |x_2|, |L - x_1|, |L - x_2|\right]$, $v = \max\left[|x_1|, |x_2|, |L - x_1|, |L - x_2|\right]$.

the 2nd pseudo-Rényi entropy (16), it's helpful to study the early and late time behaviors of η and $\bar{\eta}$ firstly, which we summarize in the table 1.[8] We can see from the table that for general

Table 1: Early time and late time behaviors of $(\eta, \bar{\eta})$ for the subsystem $A = [0, \infty)$.

$(\eta, \bar{\eta})$	$x_1 x_2 > 0$	$x_1 x_2 < 0$	
Late time $(t \to \infty)$	$(1, 0)$	$(1, 0)$	
Early time $(t \to 0)$	$\left(\frac{1}{2} + a, \frac{1}{2} + a\right)$	$x_1 > 0 > x_2$	$x_2 > 0 > x_1$
	$a = \frac{x_1 + x_2}{4\sqrt{x_1 x_2}}$	$\left(\frac{1}{2} + a, \frac{1}{2} - a\right)$	$\left(\frac{1}{2} - a, \frac{1}{2} + a\right)$

space configurations of the two inserted points, the late time behaviors of cross ratios are uniform. Still, the early time behavior is somewhat intricate. One can, however, obtain concise results by thinking about the situations where two operators are very close together. Intuitively, we may expect the results to degenerate into the case of Rényi entropy. The quadratic limit of cross ratios is given by

$$\lim_{x_1 \to x_2} \lim_{t \to 0} (\eta, \bar{\eta}) \simeq \begin{cases} (0, 0), & x_2 < 0 \\ (1, 1), & x_2 > 0 \end{cases}, \tag{19}$$

These coincide with the second Rényi entropy results in [35]. Another intriguing case is to set $x_2 = -x_1 \neq 0$, where the early time limit of cross ratios is reduced to

$$\lim_{t \to 0} (\eta, \bar{\eta}) \simeq \left(\frac{1}{2}, \frac{1}{2}\right). \tag{20}$$

We next follow the arguments in [33, 37] to cope with the function $G_{(\eta, \bar{\eta})}$ in (16). In general CFTs, $G(\eta, \bar{\eta})$ can be expressed as follows using the conformal blocks [50]

$$G(\eta, \bar{\eta}) = \sum_p (C^p_{\mathcal{O}^\dagger \mathcal{O}})^2 F_{\mathcal{O}}(p|\eta) \bar{F}_{\mathcal{O}}(p|\bar{\eta}), \tag{21}$$

where $C^p_{\mathcal{O}^\dagger \mathcal{O}}$ is the coefficient of the three-point function $\langle \mathcal{O}^\dagger \mathcal{O} \phi_p \rangle$ and the index p corresponds to each ϕ_p of all Virasoro primary fields. We can normalize $G(\eta, \bar{\eta})$ such that the two-point function (10) has a unit normalization $c_{12} = 1$, and it leads to the following behavior of $F_{\mathcal{O}}(p|\eta)$ in $\eta \to 0$ limit[9]

$$\lim_{\eta \to 0} F_{\mathcal{O}}(p|\eta) = \eta^{\Delta_p - 2\Delta_{\mathcal{O}}} (1 + O(\eta)). \tag{22}$$

The above behavior indicates that as η goes to zero, the identity operator dominates the contribution in the summation of (21). Moreover, with the bootstrap relation

$$G(\eta, \bar{\eta}) = G(1 - \eta, 1 - \bar{\eta}), \tag{23}$$

---

[8]The details of derivation can be found in appendix A.1.

[9]Note we set ϕ_0 to be equal to the identity operator, which means $\Delta_0 = 0$.

we obtain behaviors of $G(\eta, \bar{\eta})$ in two limits for general 2d CFTs

$$\lim_{\substack{\eta \to 0 \\ \bar{\eta} \to 0}} G(\eta, \bar{\eta}) \simeq |\eta|^{-4\Delta_{\mathcal{O}}}, \quad \lim_{\substack{\eta \to 1 \\ \bar{\eta} \to 1}} G(\eta, \bar{\eta}) \simeq |1 - \eta|^{-4\Delta_{\mathcal{O}}}. \tag{24}$$

The above results correspond precisely to the early time behavior of the $G(\eta, \bar{\eta})$ function when the spatial positions of the two inserted operators tend to coincide.

The late time behavior of $G(\eta, \bar{\eta})$, according to the table 1, requires some knowledge of the behavior of conformal block in the limit $\eta \to 1$. For rational CFTs, the fusion transformation [51, 52]

$$F_{\mathcal{O}}(p|1 - \eta) = \sum_q F_{pq}[\mathcal{O}] \cdot F_{\mathcal{O}}(q|\eta) \tag{25}$$

can be exploited to give the expression of $F_{\mathcal{O}}(p|\eta)$ in $\eta \to 1$ limit and thus fix the leading-order of the late time behavior of G

$$\lim_{\substack{\eta \to 1 \\ \bar{\eta} \to 0}} G(\eta, \bar{\eta}) \simeq d_{\mathcal{O}}^{-1}(1 - \eta)^{-2\Delta_{\mathcal{O}}} \bar{\eta}^{2\Delta_{\mathcal{O}}}, \tag{26}$$

where $d_{\mathcal{O}} = 1/F_{00}[\mathcal{O}]$ is the quantum dimension [52] of $\mathcal{O}$. Combine (9) with (24) and (26), we find the following expression for the second pseudo-Rényi entropy

$$\Delta S_A^{(2)} \simeq \begin{cases} 0, & t \to 0 \ \&\& \ x_1 \sim x_2, \\ \log d_{\mathcal{O}}, & t \to \infty. \end{cases} \tag{27}$$

It is noted that the late limit of both 2nd pseudo-Rényi entropy and Rényi entropy saturates to $\log d_{\mathcal{O}}$, which indicates that the quasiparticle pair picture seems to be preserved in the pseudo-entropy.

We next move to analyse large-c CFTs. For large-c CFTs, in the limit $\Delta_p/c \ll 1$, the conformal block has the following universal form [53, 54]

$$F_{\mathcal{O}}(p, \eta) \simeq \eta^{\Delta_p - 2\Delta_{\mathcal{O}}} \cdot {}_2F_1(\Delta_p, \Delta_p, 2\Delta_p; \eta), \tag{28}$$

where ${}_2F_1(a, b, c; z)$ is the hypergeometric function. Whereas, the authors in [37] argued that the above approximation fails when η is very close to 1 such as $|1 - \eta| \sim (D_{\mathcal{O}}^p)^{-\frac{1}{2\Delta_{\mathcal{O}}}}$, where $D_{\mathcal{O}}^p \sim \exp(c^\alpha)$ (α is a certain positive constant) is exponentially large and in RCFTs $D_{\mathcal{O}}^0$ coincides with the quantum dimension $d_{\mathcal{O}}$. When η is very close to 1, the leading order of $F_{\mathcal{O}}(p, \eta)$ is given by [37]

$$F_{\mathcal{O}}(p, \eta) \simeq \frac{1}{D_{\mathcal{O}}^p} \cdot (1 - \eta)^{-2\Delta_{\mathcal{O}}}, \quad \left(|1 - \eta| \lesssim (D_{\mathcal{O}}^p)^{-\frac{1}{2\Delta_{\mathcal{O}}}} \right). \tag{29}$$

Furthermore, following the arguments in [37], the summation in Eq.(21) can be approximated by counting the contribution of the conformal vacuum block

$$G(\eta, \bar{\eta}) \simeq F_{\mathcal{O}}(0, \eta) \bar{F}_{\mathcal{O}}(0, \bar{\eta}) \tag{30}$$

when we are considering large-c theroies with gravity duals. Eq.(22) with Eq.(28-30) together lead to another type of the late time limit of $G(\eta, \bar{\eta})$

$$G(\eta, \bar{\eta}) \simeq \begin{cases} \bar{\eta}^{-2\Delta_\mathcal{O}}, & |1 - \eta| \gtrsim (D_\mathcal{O}^p)^{-\frac{1}{2\Delta_\mathcal{O}}}, \\ \frac{1}{D_\mathcal{O}^0} \cdot (1 - \eta)^{-2\Delta_\mathcal{O}} \bar{\eta}^{-2\Delta_\mathcal{O}}, & |1 - \eta| \lesssim (D_\mathcal{O}^p)^{-\frac{1}{2\Delta_\mathcal{O}}}. \end{cases} \tag{31}$$

Substituting (24) and (31) into (16) respectively, We obtain three distinct stages of evolution of the second pseudo-Rényi entropy.

$$\Delta S_A^{(2)} \simeq \begin{cases} 0, & t \to 0 \text{ and } x_1 \sim x_2, \\ \log\left[\left(-\left(\frac{x_1-x_2+2i\epsilon}{4t}\right)^2\right)^{-2\Delta_\mathcal{O}}\right], & \max\left[|x_1|, |x_2|, \epsilon\right] \ll t \lesssim \frac{1}{4}(D_\mathcal{O}^0)^{\frac{1}{4\Delta_\mathcal{O}}} \sqrt{(x_1-x_2)^2+4\epsilon^2}, \\ \log D_\mathcal{O}^0, & t \gtrsim \frac{1}{4}(D_\mathcal{O}^0)^{\frac{1}{4\Delta_\mathcal{O}}} \sqrt{(x_1-x_2)^2+4\epsilon^2}. \end{cases} \tag{32}$$

Like Rényi entropy [37], the second pseudo-Rényi entropy has an intermediate process of logarithmic time evolution. If we take the real part of $\Delta S_A^{(2)}$, as we are interested in, the corresponding logarithm evolves as follows

$$\text{Re}\left[\Delta S_A^{(2)}\right] = 4\Delta_\mathcal{O} \log \frac{4t}{\sqrt{(x_1-x_2)^2+4\epsilon^2}}, \tag{33}$$

which matches the result in [37] when two space points coincide. It's rewarding to mention that when we take the large-c limit first, like in holography, $D_\mathcal{O}^0$ will go to infinity, and $\Delta S_A^{(2)}$ is left with logarithmical growth.

The subsystem $A = [0, L]$: In the case of finite scale, the early time and late time behaviors of the cross ratios can be readily obtained from the expressions of cross ratios (92) after the analytic continuation,

$$\lim_{t \to 0}(\eta, \bar{\eta}) \simeq \begin{cases} (\frac{1}{2} + b, \frac{1}{2} + b), & x_1, x_2 < 0 || 0 < x_1, x_2 < L || L < x_1, x_2, \\ (\frac{1}{2} + b, \frac{1}{2} - b), & x_1 > L > x_2 > 0 || L > x_1 > 0 > x_2, \\ (\frac{1}{2} - b, \frac{1}{2} + b), & x_2 > L > x_1 > 0 || L > x_2 > 0 > x_1, \\ (\frac{1}{2} - b, \frac{1}{2} - b), & x_1 > L > 0 > x_2 || x_2 > L > 0 > x_1, \end{cases} \left(b = \frac{L(x_1+x_2)-2x_1 x_2}{4\sqrt{x_1 x_2(L-x_1)(L-x_2)}}\right), \tag{34}$$

$$\lim_{t \to \infty}(\eta, \bar{\eta}) \simeq \left(-\frac{L^2(x_2-x_1+2i\epsilon)^2}{16t^4}, -\frac{L^2(x_2-x_1-2i\epsilon)^2}{16t^4}\right) \simeq (0, 0). \tag{35}$$

Once again, we encounter a complicated early time behavior, and it can be simplified by taking quadratic limit ($x_1 \sim x_2$ and $t \sim 0$)

$$\lim_{x_1 \to x_2} \lim_{t \to 0}(\eta, \bar{\eta}) \simeq \begin{cases} (0, 0), & x_2 < 0 || L < x_2, \\ (1, 1), & 0 < x_2 < L. \end{cases} \tag{36}$$

Furthermore, we find that another interesting class of space configurations, $|x_1|, |x_2| \gg L$, can also reduce the early time results (34),

$$\lim_{t \to 0}(\eta, \bar{\eta}) \simeq (0, 0), \quad (|x_1|, |x_2| \gg L). \tag{37}$$

To analytically extract the middle time $\big(t \in [u,v],\ u = \min\big[|x_1|,|x_2|,|L-x_1|,|L-x_2|\big],$ $v = \max\big[|x_1|,|x_2|,|L-x_1|,|L-x_2|\big]\big)$ behavior of cross ratios, let us consider the large L limit, that is, $L \gg |x_1 - x_2|$. This is because one can expect that when $L \gg |x_1 - x_2|$, the middle time behavior of $\Delta S_A^{(2)}$ will tend to the late time behavior of $\Delta S_A^{(2)}$ of the infinite subsystem. Consider two special spatial configurations that satisfy the constraint: i. $L \gg \max\big[|x_1|,|x_2|\big]$; ii. $L \gg \max\big[|L-x_1|,|L-x_2|\big]$. The above two configurations correspond to the situation where operators live concentratedly near the left and right boundaries of A, respectively.[10] In these cases, the value of the cross ratios at a typical middle time, $t = L/2$, can be calculated analytically

$$
\lim_{t \to \frac{L}{2}} (\eta, \bar{\eta}) \simeq
\begin{cases}
\left(1 + \frac{(x_2 - x_1 + 2i\epsilon)^2}{L^2}, -\frac{(x_2 - x_1 - 2i\epsilon)^2}{9L^2}\right) \simeq (1,0), & L \gg \max\big[|x_1|,|x_2|\big], \\[4mm]
\left(-\frac{(x_2 - x_1 + 2i\epsilon)^2}{9L^2}, 1 + \frac{(x_2 - x_1 - 2i\epsilon)^2}{L^2}\right) \simeq (0,1), & L \gg \max\big[|L-x_1|,|L-x_2|\big].
\end{cases}
\tag{39}
$$

We obtain a middle-time behavior similar to the late-time behavior (86) for the infinite subsystem. For more general cases, the numerical calculation shows that

$$
(\eta, \bar{\eta})\big|_{t \in [u',v']} \simeq
\begin{cases}
(1,0), & L \gg |x_1 - x_2|\ \&\&\ x_{\min} < \frac{L - |x_1 - x_2|}{2}, \\[2mm]
(0,1), & L \gg |x_1 - x_2|\ \&\&\ x_{\min} > \frac{L - |x_1 - x_2|}{2},
\end{cases}
\quad (x_{\min} \equiv \min\big[x_1, x_2\big]),
\tag{40}
$$

where $u' = \min\big[\{|x_1|,|x_2|,|L-x_1|,|L-x_2|\}\backslash\{u\}\big]$, $v' = \max\big[\{|x_1|,|x_2|,|L-x_1|,|L-x_2|\}\backslash\{v\}\big]$ for $x_1 \neq x_2$ and $[u',v'] = [u,v]$ for $x_1 = x_2$.

Combining with the previous discussion of $G(\eta, \bar{\eta})$, according to Eqs.(36), (40), and (35), we get the picture of the evolution of $\Delta S_A^{(2)}$ under some constraints in RCFTs[11]

$$
\Delta S_A^{(2)} \simeq
\begin{cases}
0, & t \sim 0\ \&\&\ \big(|x_1 - x_2| \sim 0\ ||\ L \ll |x_1|,|x_2|\big), \\[2mm]
\log d_{\mathcal{O}}, & t \in [u',v']\ \&\&\ L \gg |x_1 - x_2|\ \&\&\ x_{\min} < \frac{L - |x_1 - x_2|}{2}, \\[2mm]
\log \bar{d}_{\mathcal{O}}, & t \in [u',v']\ \&\&\ L \gg |x_1 - x_2|\ \&\&\ x_{\min} > \frac{L - |x_1 - x_2|}{2}, \\[2mm]
0, & t \to \infty.
\end{cases}
\tag{41}
$$

3.1.2 Examples in 2d CFTs

In the previous subsection, we have studied several limiting behaviors of the second pseudo-Rényi entropy. However, there are still some mysteries about the evolution of $\Delta S_A^{(2)}$ that limit analysis is infeasible to solve:

1. The intermediate process of the evolution of $\mathrm{Re}[\Delta S_A^{(2)}]$ from an initial value to $\log d_{\mathcal{O}}$ in RCFTs.

---

[10]One may also interested in the opposing situation that the operators are scattered at both ends of A. The middle time behavior of cross ratios in this case is found to be

$$
\lim_{t \to \frac{\sqrt{2}L}{2}} (\eta, \bar{\eta}) \simeq \left(\frac{1}{2} + O(1/L), \frac{1}{2} + O(1/L)\right), \quad L \gg \max\big[|x_1|,|L-x_2|\big].
\tag{38}
$$

[11]Note that normally the quantum dimension $d_{\mathcal{O}}$ is real, and this is true in all the models considered in this paper (i.e. we have $\bar{d}_{\mathcal{O}} = d_{\mathcal{O}}$ in this paper).

2. Is there anything special about $\text{Re}[\Delta S_A^{(2)}]$ evolution in certain symmetric spatial configurations (such as $x_1 = -x_2$ for $A = [0, \infty)$)?

In this subsection, we will resort to numerical analysis to uncover the whole time evolution picture of $\Delta S_A^{(2)}$ under several specific 2d CFT models. We expect that the above problems will be answered to some extent in these concrete models. Before entering into the numerical study, we first point out some model-independent symmetries of the second pseudo-Rényi entropy, which are reflected in the following examples.

Symmetries for $\Delta S_A^{(2)}$: Re-examining the cross ratios of finite and infinite subsystem ((92) and (85),respectively), one can find some hidden symmetries of them,

$$\eta(x_2, x_1, t) = \left[\eta(x_1, x_2, t)\right]^*, \quad \bar{\eta}(x_2, x_1, t) = \left[\bar{\eta}(x_1, x_2, t)\right]^*, \tag{42}$$

$$\eta(-x_1, -x_2, t) = 1 - \bar{\eta}(x_1, x_2, t), \qquad \left(A = [0, \infty)\right), \tag{43}$$

$$\eta(L - x_1, L - x_2, t) = \bar{\eta}(x_1, x_2, t), \qquad \left(A = [0, L]\right), \tag{44}$$

where " $*$ " denotes complex conjugate. Further, it's easy to show that the above symmetries may be extended to $\Delta S_A^{(2)}$ when the $G(\eta, \bar{\eta})$ function has the following properties

$$G(\eta, \bar{\eta}) = G(\bar{\eta}, \eta), \tag{45}$$

$$G(\eta^*, \bar{\eta}^*) = [G(\eta, \bar{\eta})]^*. \tag{46}$$

Combining (16), (42), and (46), one obtains the first symmetry of $\Delta S_A^{(2)}$,

$$\Delta S_A^{(2)}(x_2, x_1, t) = \begin{cases} \Delta S_A^{(2)}(x_1, x_2, t), & \text{Tr}\left[\left(\mathcal{T}_A^{1|2}(t)\right)^2\right] \in \mathbb{R}_-, \\ \left[\Delta S_A^{(2)}(x_1, x_2, t)\right]^*, & \text{Tr}\left[\left(\mathcal{T}_A^{1|2}(t)\right)^2\right] \in \mathbb{C} \setminus \mathbb{R}_-. \end{cases} \tag{47}$$

Combining (16), (23), and (43-45), the second symmetry of $\Delta S_A^{(2)}$ reads

$$\Delta S_{[0,L]}^{(2)}(x_1, x_2, t) = \Delta S_{[0,L]}^{(2)}(L - x_1, L - x_2, t), \tag{48}$$

$$\Delta S_{[0,\infty)}^{(2)}(x_1, x_2, t) = \Delta S_{[0,\infty)}^{(2)}(-x_1, -x_2, t). \tag{49}$$

There are some physical or mathematical understandings that may explain the appearance of the above symmetries. For $A = [0, L]$, both A and A^c are invariant under reflection with respect to $x = L/2$, which implies two sets of space configurations are symmetric. Thus pseudo-Rényi entropy should be equal with the inserted points (x_1, x_2) and $(L - x_1, L - x_2)$, hence we obtain (48); For $A = [0, \infty)$, we may have the equality $S_A^{(n)}(x_1, x_2, t) = S_{A^c}^{(n)}(-x_1, -x_2, t)$ in terms of the symmetry of the system. In addition to the basic property $S^{(n)}(\mathcal{T}_{A^c}^{1|2}) = S^{(n)}(\mathcal{T}_A^{1|2})$ of the nth pseudo-Rényi entropy [20], we obtain (49); Eq.(47) can be interpreted by the fact that exchanging x_1 with x_2 is equivalent to let $\mathcal{T}^{1|2}(t) \to \left(\mathcal{T}^{1|2}(t)\right)^\dagger$. The above argument suggests

11

that these symmetries hold not only for the 2nd pseudo-Rényi entropy, but also for any order. We shall make a numerical examination on them in section 4.

On the other hand, one can see that there are two special space configurations — $x_1 = L - x_2$ for $A = [0, L]$ and $x_1 = -x_2$ for $A = [0, \infty)$, that are screened out by these symmetries. Taking $x_1 = -x_2$, $A = [0, \infty)$ as an example, the operation of swapping x_1 and x_2 is equivalent to the spatial reflection operation, which means that $\Delta S_{[0,\infty)}^{(2)}(x_1, -x_1, t)$ is real when $\text{Tr}\left[\left(\mathcal{T}_{[0,\infty)}^{1|2}(t)\right)^2\right] \in \mathbb{C} \setminus \mathbb{R}_-$. For $A = [0, L]$, simple algebra shows that $\Delta S_{[0,L]}^{(2)}(x_1, L - x_1, t) = \log \frac{c_{12}^2}{|\eta(1-\eta)|^{4\Delta_{\mathcal{O}}} G(\eta, \eta^*)}$.[12] Since one can expect $G(\eta, \eta^*)$ to be greater than 0, we obtain a real second pseudo-Rényi entropy evolution in this insertion configuration, whose correctness is verified in subsequent examples.

Finally, when only paying attention to the real part of $\Delta S_A^{(2)}$, the above results show that the evolution of $\text{Re}[\Delta S_A^{(2)}]$ may be "4-fold degenerate",

$$
\begin{aligned}
\text{Re}[\Delta S_{[0,L]}^{(2)}(x_1, x_2, t)] &= \text{Re}[\Delta S_{[0,L]}^{(2)}(L - x_1, L - x_2, t)] \\
=\text{Re}[\Delta S_{[0,L]}^{(2)}(x_2, x_1, t)] &= \text{Re}[\Delta S_{[0,L]}^{(2)}(L - x_2, L - x_1, t)],
\end{aligned}
\tag{50}
$$

$$
\begin{aligned}
\text{Re}[\Delta S_{[0,\infty)}^{(2)}(x_1, x_2, t)] &= \text{Re}[\Delta S_{[0,\infty)}^{(2)}(-x_1, -x_2, t)] \\
=\text{Re}[\Delta S_{[0,\infty)}^{(2)}(x_2, x_1, t)] &= \text{Re}[\Delta S_{[0,\infty)}^{(2)}(-x_2, -x_1, t)].
\end{aligned}
\tag{51}
$$

Hence we may choose to label each space configuration with the following parameters

$$
x_m \equiv \frac{x_1 + x_2}{2}, \quad l \equiv |x_1 - x_2|.
\tag{52}
$$

Example I— Free scalar: Let us warm up with a simple example — the $c = 1$ free scalar, and choose the operator $\mathcal{O} = \frac{1}{\sqrt{2}}\left(e^{\frac{i}{2}\phi} + e^{-\frac{i}{2}\phi}\right)$ which has (chiral and antichiral) conformal dimension $\Delta_{\mathcal{O}} = \frac{1}{8}$ and quantum dimension $d_{\mathcal{O}} = 2$. The corresponding function $G(\eta, \bar{\eta})$ is found to be $G(\eta, \bar{\eta}) = \frac{1 + |\eta| + |1 - \eta|}{2\sqrt{|\eta||1 - \eta|}}$, which apparently satisfies Eqs.(45), (46) and gives the following concise expression of $\Delta S_A^{(2)}$,

$$
\Delta S_A^{(2)}(\eta, \bar{\eta}) = \log \frac{2}{1 + |\eta| + |1 - \eta|}.
\tag{53}
$$

On the other hand, utilizing the identity $\langle \sigma(z_1, \bar{z}_1)...\sigma(z_{2n}, \bar{z}_{2n}) \rangle_{\Sigma_1}^2 = \langle \mathcal{O}(z_1, \bar{z}_1)...\mathcal{O}(z_{2n}, \bar{z}_{2n}) \rangle_{\Sigma_1}$ and $\Delta_{\mathcal{O}} = 2\Delta_\sigma$ [55], where σ is the spin operator in Ising model, it can be found that $\Delta S_A^{(n)}[\mathcal{O}\text{-excitation}] = 2\Delta S_A^{(n)}[\sigma\text{-excitation}]$. Thus our calculations in this part are also applicable to the case of σ-excitation in Ising model.

Now we turn to the numerical component. The first is the simpler case that $A = [0, \infty)$. As shown in figure 2(a), since the relative size between the spacing of two operators and the

---

[12]The absolute value here is $|\eta| \equiv \sqrt{\eta \cdot \eta^*}$.
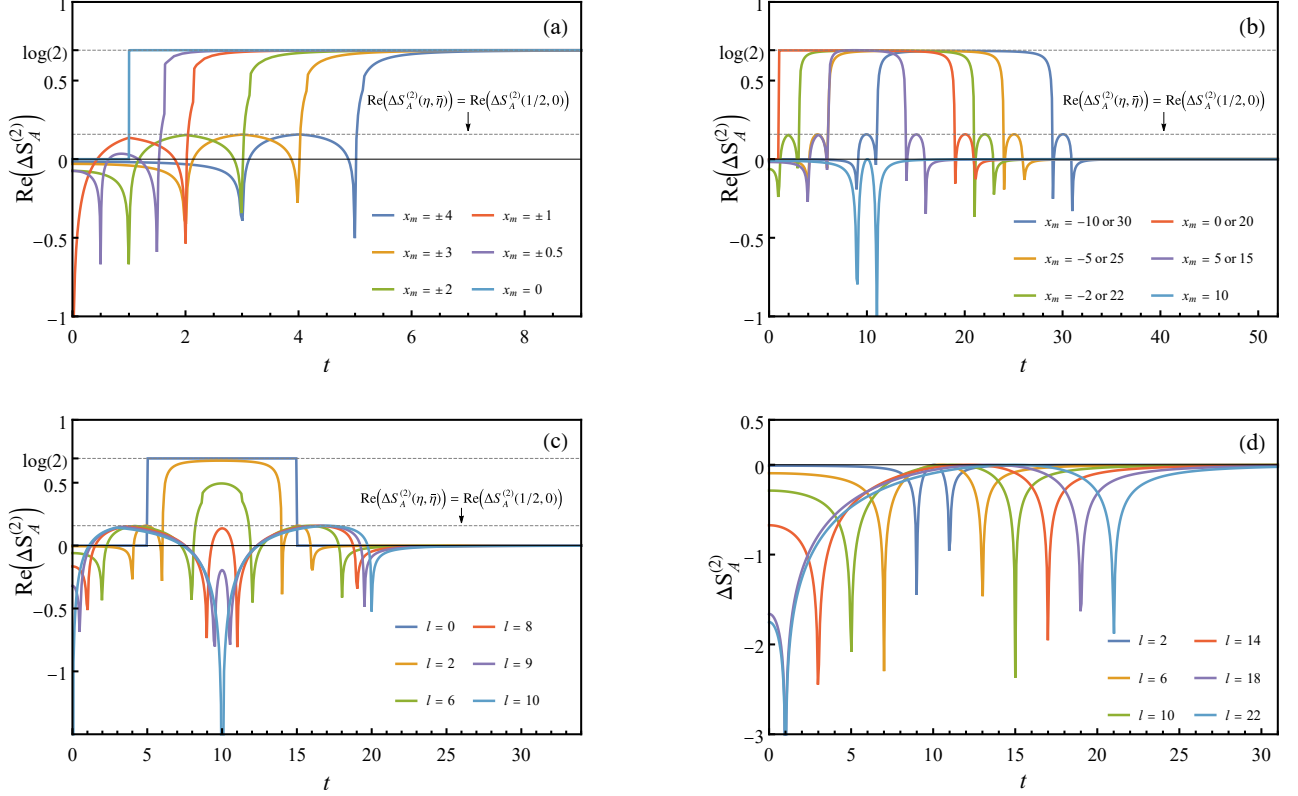
Figure 2: The real-time evolution of $\text{Re}[\Delta S_A^{(2)}]$ in $c = 1$ free scalar, where the insertion operator is chosen to be $\frac{1}{\sqrt{2}}(e^{i\phi} + e^{-i\phi})$ and the regulator $\epsilon = 10^{-5}$. (a): $A = [0, \infty)$, $l = 2$; (b): $A = [0, 20]$, $l = 2$; (c): $A = [0, 10]$, $x_m = -5$; (d): $A = [0, 20]$, $x_m = 10$.

scale of the subsystem is not involved in this case, we fix l ($l = 2$) and adjust x_m to observe the evolution of $\text{Re}[S_A^{(2)}]$. One can read a common feature from these evolving curves (except for the case of $x_m = 0$): There is a small hump between the early time evolution determined by (87) and the late time evolution determined by Eq.(86). We can explain the appearance of the hump to some extent in terms of the picture of quasiparticle propagation. Under the quasiparticle propagation picture, the time nodes at which the hump shape evolution begins and ends correspond exactly to the time nodes at which two quasiparticle pairs moving at the speed of light from the insertion points enter or leave the subsystem A. It can be found that the peak of the hump shape evolution is reached at $t \simeq |x_m|$, and the value of the cross ratios at this time is given by

$$\lim_{t \to |x_m|} (\eta, \bar{\eta}) = \begin{cases} \left(\frac{1}{2} + O(t - |x_m|), \frac{1}{2} + \frac{x_m}{\sqrt{4x_m^2 - \frac{1}{4}l^2 + \epsilon^2 - i\epsilon l}} + O(t - |x_m|) \right), & x_m < 0, \\ \left(\frac{1}{2} + \frac{x_m}{\sqrt{4x_m^2 - \frac{1}{4}l^2 + \epsilon^2 - i\epsilon l}} + O(t - |x_m|), \frac{1}{2} + O(t - |x_m|) \right), & x_m > 0. \end{cases} \tag{54}$$

Obviously $\frac{x_m}{\sqrt{4x_m^2 - \frac{1}{4}l^2 + \epsilon^2 - i\epsilon l}} \to \pm \frac{1}{2}$ when $|x_m| \gg l$, but the approximation is accurate enough when $|x_m| \geq l$. Thus we have

$$\lim_{t \to |x_m|} (\eta, \bar{\eta}) \simeq \begin{cases} \left(\frac{1}{2}, 0 \right), & x_m \leq -l, \\ \left(1, \frac{1}{2} \right), & x_m \geq l. \end{cases} \tag{55}$$

13

However, due to the symmetries of $G(\eta, \bar{\eta})$, the above two cases give the same value of $\text{Re}[S_A^{(2)}]$. For the most special case of $x_m = 0$, which we have already encountered in the limit analysis (20), $\text{Re}[S_A^{(2)}]$ behaves exactly like the second Rényi entropy [49]. In fact, we find $\Delta S_A^{(2)}$ is real in this case,

$$\Delta S_{[0,\infty)}^{(2)}(x, -x, t) = \begin{cases} 0, & 0 \le t < |x|, \\ \log 2, & t > |x|, \end{cases} \tag{56}$$

which is consistent with our previous symmetry analysis. Next, we categorize the case of $A = [0, L]$ in terms of the relative size between the spacing of two operators and the scale of the subsystem. When the distance between two operators is much smaller than the length of the subsystem (i.e. $l \ll L$), as depicted in figure 2(b), we reproduce the evolution pattern described by Eq.(41). Notice that we lost the middle time behavior of $\log d_{\mathcal{O}}$ in the case of $x_m = 10$, since in this case the related time interval (interval in Eq.(40)) is a null set. Unlike the case of the infinite subsystem, We can see that the small hump virtually appears twice in the evolving curves in figure 2(b). Again, this coincides with the picture of quasiparticle pairs propagation in a finite subsystem. The cross ratios for the peaks of the humps are found to be

$$\lim_{t \to |x_m|} (\eta, \bar{\eta}) \simeq \begin{cases} \left(\frac{1}{2}, 0\right), & L \gg l \ \&\& \ x_m \le -l, \\ \left(1, \frac{1}{2}\right), & L \gg l \ \&\& \ l \le x_m \le (L-l)/2, \\ \left(0, \frac{1}{2}\right), & L \gg l \ \&\& \ (L+l)/2 \le x_m \le L-l, \\ \left(0, \frac{1}{2}\right), & L \gg l \ \&\& \ x_m \ge L+l. \end{cases} \tag{57}$$

$$\lim_{t \to |L-x_m|} (\eta, \bar{\eta}) \simeq \begin{cases} \left(\frac{1}{2}, 0\right), & L \gg l \ \&\& \ x_m \le -l, \\ \left(\frac{1}{2}, 0\right), & L \gg l \ \&\& \ l \le x_m \le (L-l)/2, \\ \left(\frac{1}{2}, 1\right), & L \gg l \ \&\& \ (L+l)/2 \le x_m \le L-l, \\ \left(0, \frac{1}{2}\right), & L \gg l \ \&\& \ x_m \ge L+l. \end{cases} \tag{58}$$

$\text{Re}[S_A^{(2)}(\eta, \bar{\eta})]$ is equal in the above cases, on account of the symmetries of $G(\eta, \bar{\eta})$. We then gradually increase the spacing between operators such that the constraint $l \ll L$ no longer holds (see figure 2(c)). We can see that the intermediate behavior of $\log d_{\mathcal{O}}$ gradually vanishes as l increases, but the peaks of the humps seem to remain the same. Another interesting case, as we have discussed in symmetry analysis, is to fix $x_m = L/2$ and then gradually increase l. As shown in figure 2(d), we do obtain a real pseudo-Rényi entropy. Meanwhile, the result shows that the middle time behavior of $S_A^{(2)}$ tends to zero instead of $\log d_{\mathcal{O}}$, and the time to saturation of middle time behavior also shifts from $\frac{1}{2}L$ to $\frac{\sqrt{2}}{2}L$ (38) with the increase of l.

Example II—Minimal model: Another simple example is the excitation of $(2, 1)$ operator $\phi_{(2,1)}$ in the minimal models $\mathcal{M}(p, p')$ with $p > p'$. The conformal dimension and quantum dimension of the $\phi_{(2,1)}$ are well-known to be $\Delta_{(2,1)} = \frac{3p}{4p'} - \frac{1}{2}$ and $d_{(2,1)} = -2\cos\frac{\pi p}{p'}$, respectively. In addition, it has a relatively simple four-point function [56, 57] that satisfies Eqs.(45) and

(46),

$$G(\eta,\bar{\eta}) = |\eta|^{\frac{p}{p'}}|1-\eta|^{\frac{p}{p'}} \cdot \left[\frac{\sin\left(\frac{\pi p}{p'}\right)\sin\left(\frac{3\pi p}{p'}\right)}{\sin\left(\frac{2\pi p}{p'}\right)}|I_1(\eta)|^2 + \frac{\sin\left(\frac{\pi p}{p'}\right)\sin\left(\frac{\pi p}{p'}\right)}{\sin\left(\frac{2\pi p}{p'}\right)}|I_2(\eta)|^2 \right], \qquad (59)$$

where the functions $I_{1,2}$ are defined as follows

$$I_1(\eta) = \frac{\Gamma\left(\frac{3p}{p'}-1\right)\Gamma\left(1-\frac{p}{p'}\right)}{\Gamma\left(\frac{2p}{p'}\right)} \cdot {}_2F_1\left(\frac{p}{p'}, -1+\frac{3p}{p'}, \frac{2p}{p'}, \eta\right),$$

$$I_2(\eta) = \eta^{1-\frac{2p}{p'}}\frac{\Gamma\left(1-\frac{p}{p'}\right)\Gamma\left(1-\frac{p}{p'}\right)}{\Gamma\left(2-\frac{2p}{p'}\right)} \cdot {}_2F_1\left(\frac{p}{p'}, 1-\frac{p}{p'}, 2-\frac{2p}{p'}, \eta\right). \qquad (60)$$

The normalization factor c_{12} in (16) can be read off by taking the limit $z_{12} = z_{34} \to 0$ of the four-point function[13], and the result turns out to be $c_{12}^2 = \frac{\sin\left(\frac{\pi p}{p'}\right)^2}{\sin\left(\frac{2\pi p}{p'}\right)} \cdot \frac{\Gamma\left(1-\frac{p}{p'}\right)^4}{\Gamma\left(2-\frac{2p}{p'}\right)^2}$. Since the minimal models are unitary iff $p - p' = \pm 1$, below we consider only these unitary cases and use critical Ising $\mathcal{M}(4,3)$, tricritical Ising $\mathcal{M}(5,4)$, three-state Potts at criticality $\mathcal{M}(6,5)$ and so on as prototypical examples.

Now we turn to the numerical part to observe which properties of the evolution of $\Delta S_A^{(2)}$ in the free scalar are retained in the minimal models. Figure 3(a) and 3(c) demonstrate the full-time evolution of $\text{Re}[\Delta S_A^{(2)}]$ in the cases of $A = [0, L]$ ($L \gg l$) and $A = [0, \infty)$, respectively. In these two cases, it can be found that $\text{Re}[\Delta S_A^{(2)}]$ saturates to the theoretical value $\log d_{(2,1)}$ in the middle and late time, respectively, which coincides with the case of free scalar. Whereas, since figure 3(c) is drawn under the first symmetric space configuration ($x_1 = -x_2 = \pm 5$), a comparison between the corresponding curve ($x_m = 0$) in figure 2(a) shows that there are significant differences in the behavior of $\Delta S_A^{(2)}$ in two theories: i). Except for Ising model $\mathcal{M}(4,3)$, $\Delta S_A^{(2)}$ no longer remains real in the full-time evolution, which is manifest to seen in figure 3(b).[14] The trace of $(\mathcal{T}_A^{1|2})^2$ is negative over an interval except for the Ising model, which results in a complex $\Delta S_A^{(2)}$; ii). The evolution of pseudo-Rényi entropy in the case of $x_m = 0$ no longer behaves like that of Rényi entropy; Figure 3(d) exhibits the evolution of $\Delta S_A^{(2)}$ under the second symmetric space configuration $x_m = L/2$ in the case of $A = [0, L]$. As predicted by the symmetry analysis, we can see that $\Delta S_A^{(2)}$ is real throughout the time evolution. Notice that $(\eta, \bar{\eta})$ takes the value of $(1/2, 1/2)$ at the peak or valley of the middle time evolution.

Example III—Wess–Zumino–Witten model: The last example we would like to explore is the excitation of $g_\beta^\alpha(z, \bar{z})$ operator in a Wess–Zumino–Witten (WZW) model with affine Lie

---

[13]We have $\langle\phi_{(2,1)}(z_1, \bar{z}_1)\phi_{(2,1)}(z_2, \bar{z}_2)\phi_{(2,1)}(z_3, \bar{z}_3)\phi_{(2,1)}(z_4, \bar{z}_4)\rangle \to c_{12}^2|z_{12}|^{-8\Delta_{(2,1)}}$ in the limit of $z_{12} = z_{34} \to 0$.

[14]Note that the complex $\Delta S_A^{(2)}$ is not contradictory with the previous symmetry analysis, because by symmetry analysis we can only prove that $\text{Tr}[(\mathcal{T}_A^{1|2})^2]$ is real in the case of $A = [0, \infty]$.
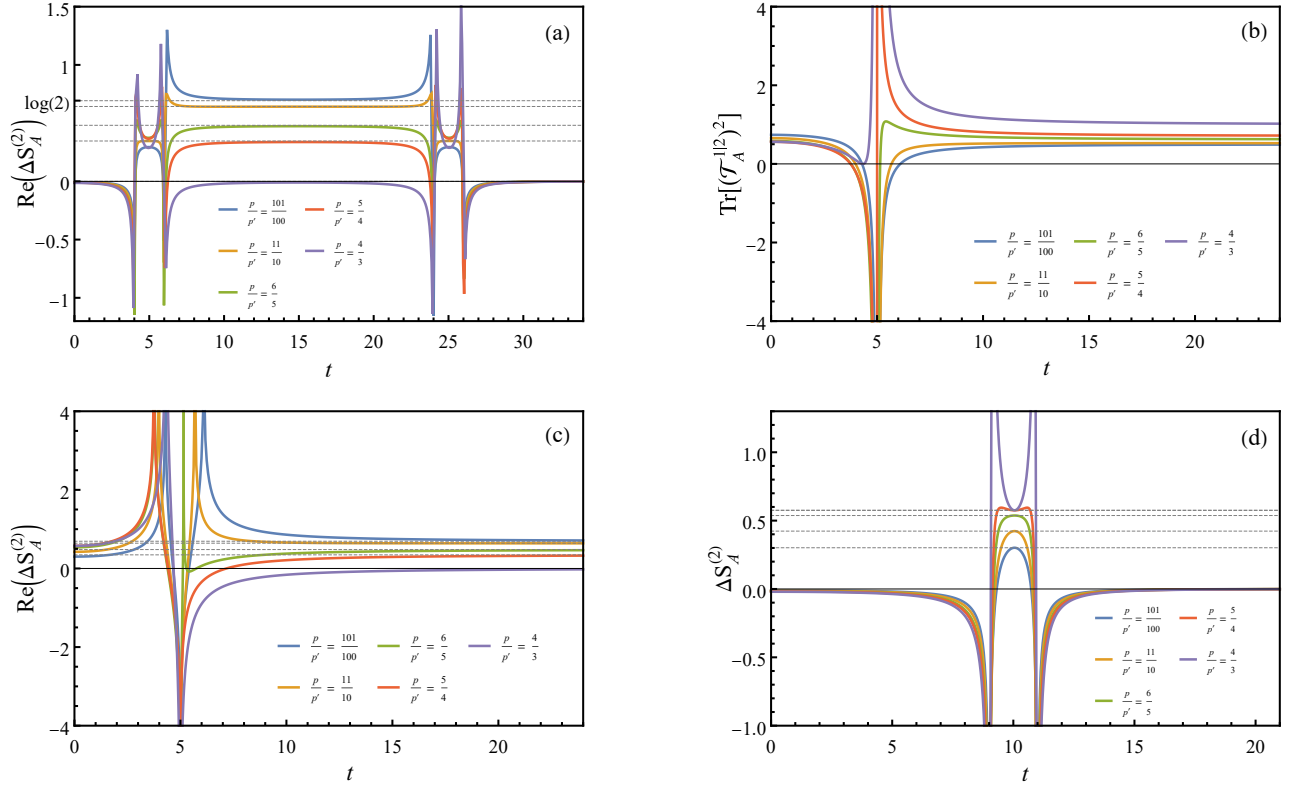
Figure 3: (a) and (c): The time evolution of $\mathrm{Re}[\Delta S_A^{(2)}]$ under the $\phi_{(2,1)}$-excitation in minimal models. The regulator is chosen to be $\epsilon = 10^{-5}$. We have $A = [0, 20]$, $l = 2$, $x_m = -5$ for (a), and $A = [0, \infty)$, $x_m = 0$, $l = 10$ for (c). The dashed line from the bottom up corresponding $\log[-2\cos(5\pi/4)]$, $\log[-2\cos(6\pi/5)]$, $\log[-2\cos(11\pi/10)]$, $\log[-2\cos(101\pi/100)]$; (b): The time evolution of $\mathrm{Tr}[(\mathcal{T}_A^{1|2})^2]$ in the case of $A = [0, \infty)$. The parameters are selected as $\epsilon = 10^{-5}$, $x_m = 0$, $l = 10$; (d): The time evolution of $\Delta S_A^{(2)}$ in the case of $A = [0, L]$. The parameters are selected as $L = 20$, $\epsilon = 10^{-5}$, $x_m = 10$, $l = 2$. $\Delta S_A^{(2)}(\eta, \bar{\eta}) = \Delta S_A^{(2)}(1/2, 1/2)$ at the dashed lines.

algebra $\mathrm{SU}(N)_k$. The operator $g_\beta^\alpha(z, \bar{z})$ in the fundamental representation $\alpha = \{1, 0, ..., 0\}$ has the (chiral and antichiral) conformal dimension $\Delta_g = \frac{N^2-1}{2N\kappa}$ and quantum dimension $d_g = N^{-1} \cdot \frac{\Gamma(1/\kappa)\Gamma(-1/\kappa)}{\Gamma(N/\kappa)\Gamma(-N/\kappa)}$, where $\kappa \equiv N + k$. The four-point function of g_β^α and its Hermitian conjugates is the solution of the well-known Knizhnik-Zamolodchikov equations [58]

$$
\begin{aligned}
&\left\langle g_\beta^\alpha(z_1, \bar{z}_1) \left(g_\beta^\alpha(z_2, \bar{z}_2)\right)^\dagger g_\beta^\alpha(z_3, \bar{z}_3) \left(g_\beta^\alpha(z_4, \bar{z}_4)\right)^\dagger \right\rangle_{\Sigma_1} \\
&= \left\langle g_\beta^\alpha(z_1, \bar{z}_1)(g^{-1})_\alpha^\beta(z_2, \bar{z}_2) g_\beta^\alpha(z_3, \bar{z}_3)(g^{-1})_\alpha^\beta(z_4, \bar{z}_4) \right\rangle_{\Sigma_1} \\
&= |z_{13} z_{24}|^{-4\Delta_g} \sum_{i,j,n=1,2} X_{nn} \mathcal{F}_i^{(n)}(\eta) \mathcal{F}_j^{(n)}(\bar{\eta}),
\end{aligned}
\tag{61}
$$
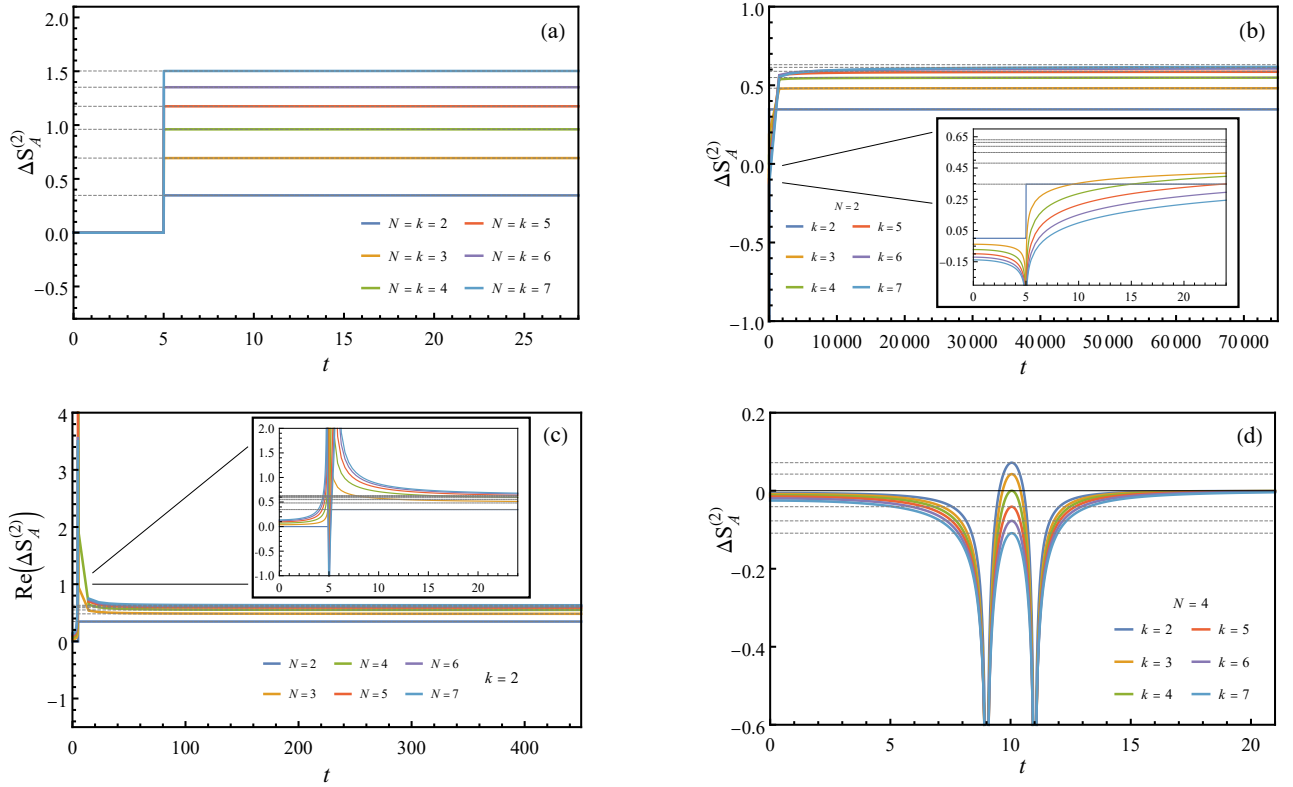
Figure 4: The real-time evolution of $\mathrm{Re}[\Delta S_A^{(2)}]$ or $\Delta S_A^{(2)}$ in $SU(N)_k$ WZW models with g_β^α-excitation. The regulator is chosen to be $\epsilon = 10^{-5}$. (a), (b), (c): $A = [0, \infty)$, $l = 10$, $x_m = 0$. The dashed lines correspond to $\log d_g$ for different N and k; (d): $A = [0, 20]$, $x_m = 10$, $l = 2$. $\Delta S_A^{(2)}(\eta, \bar{\eta}) = \Delta S_A^{(2)}(1/2, 1/2)$ at the dashed lines.

where

$$X_{11} = 1, \quad X_{22} = \frac{\Gamma\left(\frac{N+1}{\kappa}\right) \Gamma\left(\frac{N-1}{\kappa}\right) \Gamma\left(\frac{k}{\kappa}\right) \Gamma\left(\frac{k}{\kappa}\right)}{N^2 \cdot \Gamma\left(\frac{k+1}{\kappa}\right) \Gamma\left(\frac{k-1}{\kappa}\right) \Gamma\left(\frac{N}{\kappa}\right) \Gamma\left(\frac{N}{\kappa}\right)},$$

$$\mathcal{F}_1^{(1)}(\eta) = \eta^{-2\Delta_g}(1-\eta)^{\frac{N}{\kappa}-2\Delta_g} \cdot {}_2F_1\left(1/\kappa, -1/\kappa, 1 - N/\kappa; \eta\right),$$

$$\mathcal{F}_2^{(1)}(\eta) = \frac{1}{k}\eta^{1-2\Delta_g}(1-\eta)^{\frac{N}{\kappa}-2\Delta_g} \cdot {}_2F_1\left(1 + 1/\kappa, 1 - 1/\kappa, 2 - N/\kappa; \eta\right),$$

$$\mathcal{F}_1^{(2)}(\eta) = \eta^{\frac{N}{\kappa}-2\Delta_g}(1-\eta)^{\frac{N}{\kappa}-2\Delta_g} \cdot {}_2F_1\left((N-1)/\kappa, (N+1)/\kappa, 1 + N/\kappa; \eta\right),$$

$$\mathcal{F}_2^{(2)}(\eta) = -N\eta^{\frac{N}{\kappa}-2\Delta_g}(1-\eta)^{\frac{N}{\kappa}-2\Delta_g} \cdot {}_2F_1\left((N-1)/\kappa, (N+1)/\kappa, N/\kappa; \eta\right). \tag{62}$$

We next explore the full-time evolution behavior of $\Delta S_A^{(2)}$ utilizing the above information. Particularly, we are mainly concerned with the behavior of $\Delta S_A^{(2)}$ evolution under the two symmetric space configurations, i.e. $x_m = 0$ for $A = [0, \infty)$ and $x_m = L/2$ for $A = [0, L]$. As shown in figure 4, we can see that in the case of $x_m = 0$, $A = [0, \infty)$, there are three evolution patterns of $\mathrm{Re}[\Delta S_A^{(2)}]$ determined by the relative size of the rank N and level k. When $N \leq k$ (see figure 4(a) and (b)), we find that $\mathrm{Tr}[(\mathcal{T}_A^{1|2}(t))^2]$ is always greater than 0, thus $\Delta S_A^{(2)}$ remains real in the full-time evolution. A rather fascinating situation is that $N = k$, since again we observe a pseudo-Rényi entropy evolution identical to that of Rényi entropy. When $N > k$, the 2nd pseudo-Rényi entropy evolution behavior is similar to that in the minimal model. Since $\mathrm{Tr}[(\mathcal{T}_A^{1|2}(t))^2]$ is less than 0 near $t = l/2$, we have a complex pseudo entropy of in

a certain interval. Figure 4(d) depicts the behaviors of $S_A^{(2)}$ under the second symmetric space configuration $x_m = L/2$ in $A = [0, L]$. Notice that no matter k is greater than N or not, we obtain a pseudo-Rényi entropy that remains real throughout time evolution.

summaries of the above results: Let us take a short stay to briefly summarize the above results and try to answer the questions posed at the beginning of the section.

1. In general, there are one or two hump evolutions (for example, figure 2(a), (b)) between the early time and late time evolution of $\Delta S_A^{(2)}$, and the value of $\Delta S_A^{(2)}$ at the peaks of humps is $\Delta S_A^{(2)}(\eta, \bar{\eta}) = \Delta S_A^{(2)}(\frac{1}{2}, 0)$.

2. We find two special spatial configurations of operators, $x_1 = -x_2$ for $A = [0, \infty)$ and $x_1 = L - x_2$ for $A = [0, L]$, in which the the trace of $\left(\mathcal{T}_A^{1|2}(t)\right)^2$ always remains real. Within them, for the case of $x_1 = L - x_2$, we expect $\mathrm{Tr}\left[\left(\mathcal{T}_A^{1|2}(t)\right)^2\right]$ to be greater than 0, resulting in a real $\Delta S_A^{(2)}$, which is consistent with all the numerical results.

3. In the $e^{\frac{i}{2}\phi} + e^{-\frac{i}{2}\phi}$-excitation of free scalar and g_β^α-excitation of SU$(N)_k$ WZW models ($N = k$), we observe that the 2nd pseudo-Rényi entropy exhibits the same behavior as Rényi entropy in the case of $x_1 = -x_2$, $A = [0, \infty)$, i.e.

$$\Delta S_{[0,\infty)}^{(2)}(x_1, -x_1, t) = \begin{cases} 0, & 0 \le t < |x_1|, \\ \log d, & t > |x_1|. \end{cases} \tag{63}$$

3.2 Linear combination of operators

In the previous subsection, we study the real-time behaviors of $\Delta S_A^{(2)}$ for states excited by the same primary operator. It's not so straightforward to extend the results to two different primary operators. Simply substituting one of the operators would probably make a non-normalizable transition matrix since the two-point function for two different primary operators is likely to be zero. One feasible way is to consider the linear combinations of operators.[15] Consider a real-time dependent transition matrix $\mathcal{T}^{\psi|\tilde{\psi}}(t) = \frac{e^{-iHt}|\psi\rangle\langle\tilde{\psi}|e^{iHt}}{\langle\tilde{\psi}|\psi\rangle}$ consisting of two quantum states $|\psi\rangle$ and $|\tilde{\psi}\rangle$,

$$|\psi\rangle := \frac{1}{\sqrt{\langle\mathcal{O}^\dagger(x,\epsilon)\mathcal{O}(x,-\epsilon)\rangle}}\mathcal{O}(x,-\epsilon)|\Omega\rangle, \quad |\tilde{\psi}\rangle := \frac{1}{\sqrt{\langle\tilde{\mathcal{O}}^\dagger(\tilde{x},\epsilon)\tilde{\mathcal{O}}(\tilde{x},-\epsilon)\rangle}}\tilde{\mathcal{O}}(\tilde{x},-\epsilon)|\Omega\rangle,$$

$$\mathcal{O}(x,-\epsilon) = \sum_p C_p \mathcal{O}_p(x,-\epsilon), \qquad\qquad \tilde{\mathcal{O}}(\tilde{x},-\epsilon) = \sum_p \tilde{C}_p \mathcal{O}_p(\tilde{x},-\epsilon). \tag{64}$$

In the above, $\mathcal{O}(x,\epsilon) \equiv e^{\epsilon H}\mathcal{O}(x)e^{-\epsilon H}$, $\mathcal{O}_p$ are primary or descendant operators that are orthogonal to each other in the sense of the two-point function, $C_p (\tilde{C}_p)$ are superposition coefficients used to give a non-zero inner product.

---

[15]We thank Tadashi Takayanagi for bringing this idea to our attention.

3.2.1 The expected late time limit of $\Delta S_A^{(n)}$

Let's focus on the case where $A = [0, \infty)$, we expect the late time limit of $\Delta S_A^{(n)}$ to take the following form

$$\lim_{t \to \infty} \Delta S^{(n)}[\mathcal{T}_A^{\psi|\tilde{\psi}}(t)] = \frac{1}{1-n} \log \left[\sum_p \left(\frac{C_p \tilde{C}_p^* \langle \mathcal{O}_p^\dagger(\tilde{w}, \bar{\tilde{w}}) \mathcal{O}_p(w, \bar{w}) \rangle}{\sum_{p'} C_{p'} \tilde{C}_{p'}^* \langle \mathcal{O}_{p'}^\dagger(\tilde{w}, \bar{\tilde{w}}) \mathcal{O}_{p'}(w, \bar{w}) \rangle} \right)^n e^{(1-n)S^{(n)}[\mathcal{O}_p]} \right], \quad (65)$$

where $w = x - i\epsilon$, $\tilde{w} = \tilde{x} + i\epsilon$, and $S^{(n)}[\mathcal{O}_p]$ is the late time limit of the difference of entanglement entropy of $\mathcal{O}_p$-excitation ($S^{(n)}[\mathcal{O}_p] = \log d_p$ in RCFTs). It is difficult to utilize replica trick to prove Eq.(65). Nevertheless, we can provide a quantum mechanical derivation from another perspective, which as far as we know was first introduced in [42].[16] We next numerically examine the correctness of Eq.(65) using the replica trick in the concrete model.

3.2.2 Example in critical Ising

We would like to compute $\Delta S_A^{(2)}$ of linear combination operators in the critical Ising model to examine Eq.(65). There are three primary operators in the Ising model at a critical point, namely the identity $\mathbb{I}$, the spin σ, and the energy density ε. The fusion rule of them is well-known,

$$\varepsilon \times \varepsilon = \mathbb{I}, \quad \sigma \times \sigma = \mathbb{I} + \varepsilon, \quad \sigma \times \varepsilon = \sigma. \quad (66)$$

For simplicity, below, we consider the combination of σ and $\mathbb{I}$ as a typical example.

Example—$\sigma+\mathbb{I}$: Let us first define two linear combination operators

$$\mathcal{O}(w, \bar{w}) \equiv C_\sigma \cdot \sigma(w, \bar{w}) + C_\mathbb{I} \cdot \mathbb{I}, \quad \tilde{\mathcal{O}}(\tilde{w}, \bar{\tilde{w}}) \equiv \tilde{C}_\sigma \cdot \sigma(\tilde{w}, \bar{\tilde{w}}) + \tilde{C}_\mathbb{I} \cdot \mathbb{I}. \quad (67)$$

According to the fusion rule and (9), only four- and two-point functions of σ are involved in the calculation,

$$\langle \sigma(z_1, \bar{z}_1) \sigma(z_2, \bar{z}_2) \rangle_{\Sigma_1} = \frac{1}{|z_{12}|^{1/4}},$$

$$\langle \sigma(z_1, \bar{z}_1) \sigma(z_2, \bar{z}_2) \sigma(z_3, \bar{z}_3) \sigma(z_4, \bar{z}_4) \rangle_{\Sigma_1} = \left(\frac{1}{2} \left| \sqrt{\frac{z_{14} z_{23}}{z_{12} z_{34} z_{13} z_{24}}} \right| + \frac{1}{2} \left| \sqrt{\frac{z_{13} z_{24}}{z_{12} z_{34} z_{14} z_{23}}} \right| \right.$$

$$\left. + \frac{1}{2} \left| \sqrt{\frac{z_{12} z_{34}}{z_{13} z_{24} z_{14} z_{23}}} \right| \right)^{\frac{1}{2}}. \quad (68)$$

In addition, since in general $\Delta S_A^{(2)}$ of the mixed operator cannot be written as a function of cross ratios, we choose to use the following coordinates mapping between $(w, \bar{w})$ on Σ_2 and

---

[16]The derivation is presented in appendix B.

$(z, \bar{z})$ on Σ_1 [33] to complete the analytic continuation of time,

$$z_1 = \sqrt{w_1} = i\sqrt{-x_1 - t + i\epsilon}, \quad \bar{z}_1 = \sqrt{\bar{w}_1} = -i\sqrt{-x_1 + t - i\epsilon}, \tag{69}$$

$$z_2 = \sqrt{w_2} = i\sqrt{-x_2 - t - i\epsilon}, \quad \bar{z}_2 = \sqrt{\bar{w}_2} = -i\sqrt{-x_2 + t + i\epsilon}. \tag{70}$$

We start with the case of $\{\tilde{C}_p\} \neq \{C_p\}$ and $\tilde{x} = x$. An efficient way is to set $C_\sigma = q \in [0, 1]$, $C_{\mathbb{I}} = 1 - q$, $\tilde{C}_\sigma = q^k$, $\tilde{C}_{\mathbb{I}} = 1 - q^k$, and obviously what we will obtain when $k \neq 1$ is pseudo-Rényi entropy rather than Rényi entropy. Figure 5(a) shows the behavior of the late time limits of $\Delta S_A^{(2)}$ when we adjust the mixed coefficient q. We can see that the late time limits of $\Delta S_A^{(2)}$ obtained by replica method numerically (square points) are in good agreement with the results (solid lines) given by Eq.(65). With the increase of q, the contribution of σ operator gradually increases, which leads to the saturation value of 2nd (pseudo-) Rényi entropy gradually shifting from 0 ($\log d_{\mathbb{I}}$) to $\log \sqrt{2}$ ($\log d_\sigma$). Except for the late time limit, it's also intriguing to depict the the full-time evolution of $\Delta S_A^{(2)}$, see figure 5(b). We find that although $\Delta S_A^{(2)}$ saturates to a real value, globally $\Delta S_A^{(2)}$ is complex in all cases except $k = 1$ (the case of Rényi entropy).
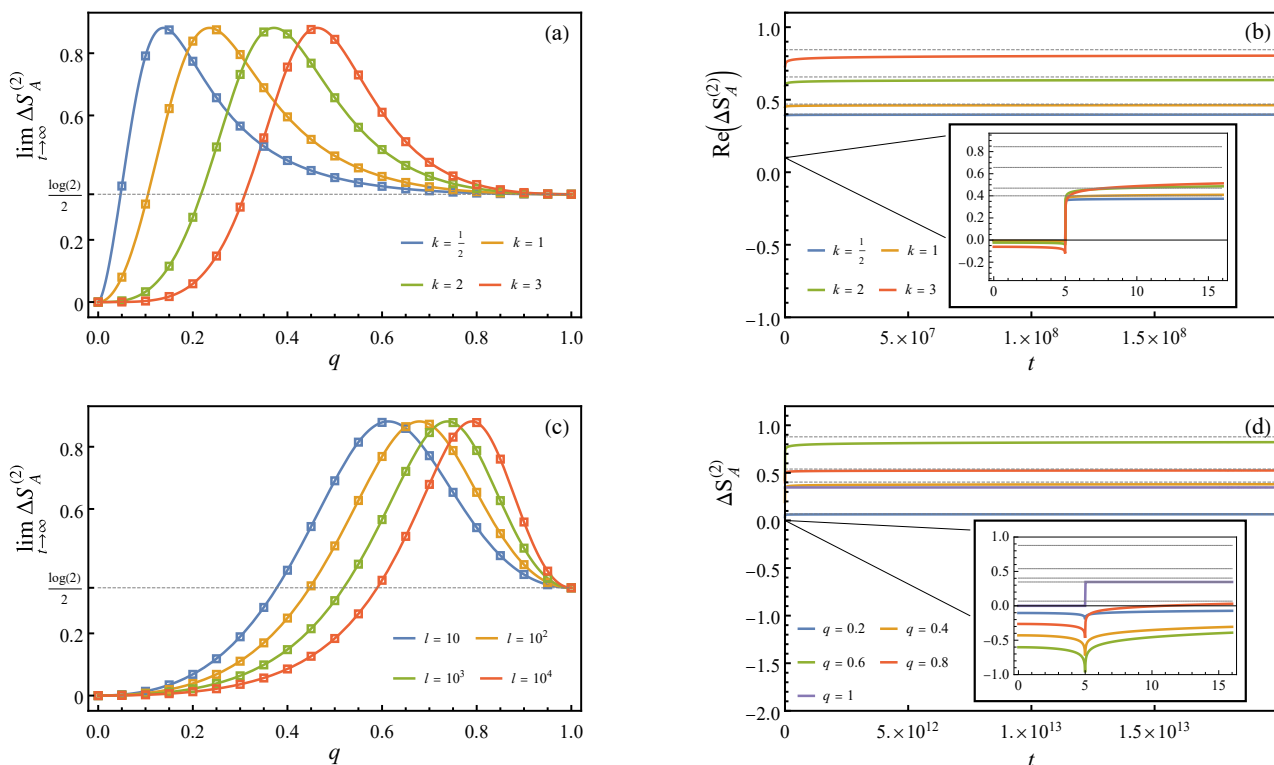
Figure 5: (a) and (c): The saturation value of $\Delta S_A^{(2)}$ in $\sigma + \mathbb{I}$-excitation. The regulator is chosen to be $\epsilon = 10^{-5}$; (b): The full-time evolution of $\mathrm{Re}[\Delta S_A^{(2)}]$ in $\sigma + \mathbb{I}$-excitation. Parameters are selected as $x = \tilde{x} = -5$, $\epsilon = 10^{-5}$. The dashed lines are the theoretical limits derived from Eq.(65) for the corresponding parameters.; (d): The full-time evolution of $\Delta S_A^{(2)}$ in $\sigma + \mathbb{I}$-excitation. Parameters are selected as $x = -\tilde{x} = \pm 5$, $\epsilon = 10^{-5}$. The dashed lines are the theoretical limits derived from Eq.(65) for the corresponding parameters.

The other interesting case we shall investigate is that $\{\tilde{C}_p\} = \{C_p\}$, $\tilde{x} \neq x$. Let us set $\tilde{C}_\sigma = C_\sigma = q$, $\tilde{C}_{\mathbb{I}} = C_{\mathbb{I}} = 1 - q$. According to (65), since $\langle \mathcal{O}_p^\dagger(\tilde{w}, \bar{\tilde{w}}) \mathcal{O}_p(w, \bar{w}) \rangle = \left((\tilde{x} - x)^2 + 4\epsilon^2\right)^{-2\Delta_p}$,

only the information of the distance of two space points $l \equiv |\tilde{x} - x|$ is related. We then plot the change of saturation value of $\Delta S_A^{(2)}$ with q under different l, as depicted in figure 5(c). Once again, we find that the theoretical value (solid lines) given by Eq.(65) is consistent with the numerical result (square points) given by replica trick. On the other hand, when the insertion point is symmetric about the origin, i.e. $\tilde{x} = -x$, $\Delta S_A^{(2)}$ is found to be real throughout the the time evolution (see figure 5(d)), which is consistent with the previous symmetry analysis.

4   General arguments and examples on $\Delta S_A^{(n)}$

In the previous section, we study the real-time behavior of $\Delta S_A^{(2)}$ for two insertion operators with different spatial coordinates. Meanwhile, we propose a formula to describe the late time limit of $\Delta S_A^{(n)}$ of linear combination operators. However, as shown in appendix B, its rationality also depends on the behavior of nth pseudo-Rényi entropy of a single primary operator insertion. Therefore, in this section, we shall quest for the properties of $\Delta S_A^{(n)}$ for two operators with different space points in the light of the results of $\Delta S_A^{(2)}$ that we have found before.

Late time limit of $\Delta S_A^{(n)}$:   The excess of nth pseudo-Rényi entropy of the reduced transition matrix $\mathcal{T}_A^{1|2}(t)$ (17) can be obtain from Eq.(7) by computing the $2n$-point function on the replica manifold Σ_n. Our primary purpose is to explore the existence of the late time saturation value of $\log d_{\mathcal{O}}$ in pseudo-Rényi entropy of higher-order when the subsystem $A = [0, \infty)$. Hence we employ the conformal map (13) to obtain the coordinates of $2n$ operators on Σ_1 first,

$$
\begin{aligned}
z_{2k+1} &= e^{2\pi i \frac{k+1/2}{n}}(-x_1 - t + i\epsilon)^{\frac{1}{n}}, \quad \bar{z}_{2k+1} = e^{-2\pi i \frac{k+1/2}{n}}(-x_1 + t - i\epsilon)^{\frac{1}{n}}, \\
z_{2k+2} &= e^{2\pi i \frac{k+1/2}{n}}(-x_2 - t - i\epsilon)^{\frac{1}{n}}, \quad \bar{z}_{2k+2} = e^{-2\pi i \frac{k+1/2}{n}}(-x_2 + t + i\epsilon)^{\frac{1}{n}}, \quad (k = 0, ..., n-1). \quad (71)
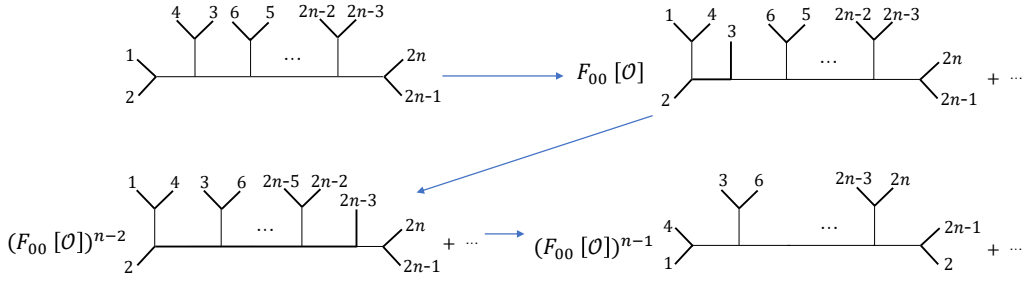\end{aligned}
$$

Then we have

$$
\frac{\langle \mathcal{O}^\dagger(w_{2n}, \bar{w}_{2n})\mathcal{O}(w_{2n-1}, \bar{w}_{2n-1})...\mathcal{O}(w_1, \bar{w}_1)\rangle_{\Sigma_n}}{\langle \mathcal{O}^\dagger(w_2, \bar{w}_2)\mathcal{O}(w_1, \bar{w}_1)\rangle_{\Sigma_1}^n} = \mathcal{C}_n \cdot \langle \mathcal{O}^\dagger(z_{2n}, \bar{z}_{2n})\mathcal{O}(z_{2n-1}, \bar{z}_{2n-1})...\mathcal{O}(z_1, \bar{z}_1)\rangle_{\Sigma_1},
$$
$$
(72)
$$

where

$$
\begin{aligned}
\mathcal{C}_n &\equiv \left(\frac{(x_1 - x_2)^2 + 4\epsilon^2}{n^2}\right)^{2n\Delta_{\mathcal{O}}} \times \prod_{i=1}^{2n}(z_i^{n-1}\bar{z}_i^{n-1})^{-\Delta_{\mathcal{O}}} \\
&\simeq \left(\frac{(x_2 - x_1)^2 + 4\epsilon^2}{n^2}\right)^{2n\Delta_{\mathcal{O}}} \times t^{4(1-n)\Delta_{\mathcal{O}}} + \text{sub-leading order terms} \quad (73) \\
&\simeq 0 \quad (t \to \infty).
\end{aligned}
$$

On the other hand, we find that at the late time $(t \to \infty)$

$$
\begin{aligned}
\lim_{t \to \infty}(z_{2(k+1)+2} - z_{2k+1}) &\simeq \frac{x_2 - x_1 + 2i\epsilon}{nt}e^{2\pi i \frac{k+1}{n}}t^{\frac{1}{n}} \simeq 0, \\
\lim_{t \to \infty}(\bar{z}_{2k+2} - \bar{z}_{2k+1}) &\simeq \frac{x_1 - x_2 + 2i\epsilon}{nt}e^{-2\pi i \frac{k+1/2}{n}}t^{\frac{1}{n}} \simeq 0, \quad (k = 0, ..., n-1; \ z_{2n+2} \equiv z_{2n}). \quad (74)
\end{aligned}
$$

Figure 6: The fusion transformations to obtain $\Delta S_A^{(n)}$.

The above results enable us to factorize the $2n$-point function $\langle \mathcal{O}^\dagger(z_{2n}, \bar{z}_{2n})...\mathcal{O}(z_1, \bar{z}_1)\rangle_{\Sigma_1}$ into n-point functions by using the fusion transformation (25) $n-1$ times (see figure 6),

$$
\langle \mathcal{O}^\dagger(z_{2n}, \bar{z}_{2n})...\mathcal{O}(z_1, \bar{z}_1)\rangle_{\Sigma_1}
$$

$$
\simeq (F_{00}[\mathcal{O}])^{n-1} \times \left(\prod_{k=0}^{n-1} (z_{2k+4} - z_{2k+1})(\bar{z}_{2k+2} - \bar{z}_{2k+1}) \right)^{-2\Delta_\mathcal{O}} + \text{sub-leading order terms}
$$

$$
\simeq (F_{00}[\mathcal{O}])^{n-1} \times \left(\frac{(x_2 - x_1)^2 + 4\epsilon^2}{n^2} \right)^{-2n\Delta_\mathcal{O}} \times t^{4(n-1)\Delta_\mathcal{O}} + \text{sub-leading order terms} \tag{75}
$$

Substituting (73) and (75) into the r.h.s. of Eq.(72), it's easy to find that the leading-order contribution at late time is $(F_{00}[\mathcal{O}])^{n-1} = d_\mathcal{O}^{1-n}$. In this way, we obtain the late time value of $\Delta S_A^{(n)}$

$$
\lim_{t\to\infty} \Delta S_A^{(n)} = \log d_\mathcal{O}. \tag{76}
$$

Symmetries of $\Delta S_A^{(n)}$: The second intention in this section is to investigate whether the symmetries found in second pseudo-Rényi entropy, i.e. Eq.(47-49), still hold in higher-order or not. It may be difficult to verify analytically, but the numerical examination is easy to take. One good object of study is the σ-excitation in the critical Ising model, since the $2n$-point function of the spin operator σ is well-known [55, 59],

$$
\langle \sigma(z_1, \bar{z}_1)...\sigma(z_{2n}, \bar{z}_{2n})\rangle_{\Sigma_1} = \frac{1}{2^n} \sum_{\substack{\varepsilon_i=\pm 1 \\ \sum \varepsilon_i=0}} \prod_{\substack{i=1,...,2n \\ i<j}} |z_i - z_j|^{\varepsilon_i \varepsilon_j/2}. \tag{77}
$$

With the help of (71) and (77), we can study the evolution behavior of $\Delta S_A^{(n)}$ under the first symmetric space configuration, i.e. $x_1 = -x_2$, $A = [0, \infty)$. On the other hand, for the second symmetric space configuration of $x_1 = L - x_2$ in $A = [0, L]$, the coordinates of 2n operators on Σ_1 will change to the following form

$$
z_{2k+1} = e^{\frac{2\pi ik}{n}} \left(\frac{x_1 + t - i\epsilon}{x_1 + t - i\epsilon - L} \right)^{\frac{1}{n}}, \quad \bar{z}_{2k+1} = e^{-\frac{2\pi ik}{n}} \left(\frac{x_1 - t + i\epsilon}{x_1 - t + i\epsilon - L} \right)^{\frac{1}{n}},
$$

$$
z_{2k+2} = e^{\frac{2\pi ik}{n}} \left(\frac{x_2 + t + i\epsilon}{x_2 + t + i\epsilon - L} \right)^{\frac{1}{n}}, \quad \bar{z}_{2k+2} = e^{-\frac{2\pi ik}{n}} \left(\frac{x_2 - t - i\epsilon}{x_2 - t - i\epsilon - L} \right)^{\frac{1}{n}}, \quad (k = 0, ..., n-1). \tag{78}
$$

Figure 7 demonstrates all situations that we are interested in. We find that the symmetries (47-49) also hold in the higher-order pseudo-Rényi entropy. It can be clearly seen from figure 7(b) and (d). Because we know that the establishment of(47-49) may bring about a real $\Delta S_A^{(n)}$ evolution. Another interesting finding is that (b) shows that the evolution of higher-order pseudo-Rényi entropy of σ-excitation under the first symmetric space configuration still maintains the evolution pattern described by (63).[17] We can also explore the asymmetric cases, as shown in (a) and (c), and there are two points worth noting: i). The higher-order pseudo-Rényi entropy in asymmetric space configuration still has hump evolution, and its peak value changes with n; ii). Figure 7(c) suggests that after the relative sizes of L and l are fixed, the middle time behavior of $\log d$ will gradually disappear with the increase of n.
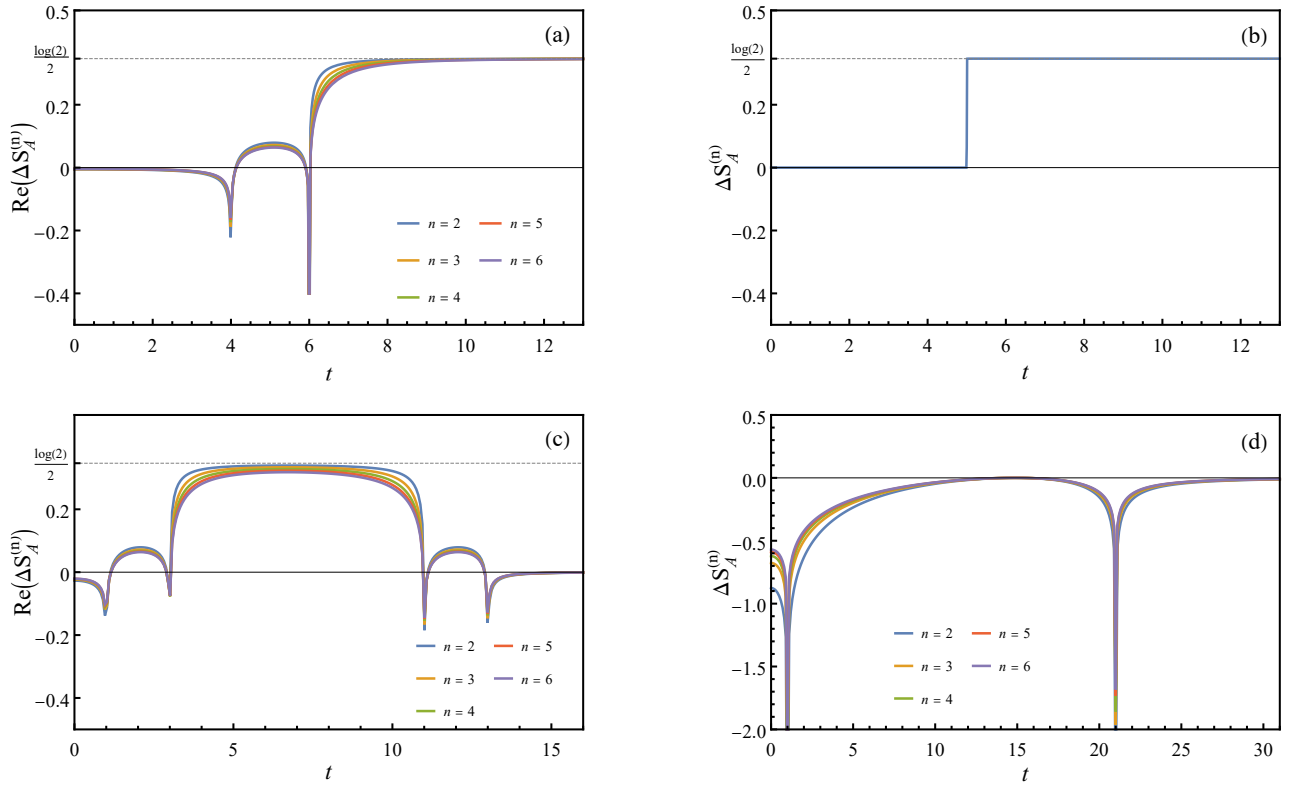
Figure 7: The real-time evolution of $\text{Re}[\Delta S_A^{(n)}]$ or $\Delta S_A^{(n)}$ for σ-excitation in critical Ising model. The regulator $\epsilon = 10^{-5}$. (a): $A = [0, \infty)$, $x_m = \pm 5$, $l = 2$; (b): $A = [0, \infty)$, $x_m = 0$, $l = 10$; (c): $A = [0, 10]$, $x_m = -2$, $l = 2$; (d): $A = [0, 20]$, $x_m = 10$, $l = 22$.

5 Conclusions and prospect

In this work, we study a generalized version of entanglement entropy and Rényi entropy, which are so-called pseudo-entropy (PE) and pseudo-Rényi entropy (PRE), respectively, in 2d CFTs. In particular, the real-time evolution of PRE associated with two locally excited states has been evaluated in various 2d CFTs, e.g., free bosonic field theory, critical Ising model, WZW model

---

[17]Due to the increasing computational complexity, we verify this point up to $n = 7$.

as well as large-c CFTs. These locally excited states are generated by acting local operators on the vacuum state, and these operators can be a single primary operator or a linear combination of them. Some fascinating behaviors of PRE evolution are found as follows:

For the reduced transition matrix generated by two primary operators with different spatial coordinates (17), we show that when subsystem A has an infinite length, the late time value of 2nd PRE is logarithmically divergent in large-c CFTs (take the large c limit first). The late time value of nth PRE saturates to $\log d$ in RCFTs (for Example, see figure 7(a)), where d is the quantum dimension of the corresponding primary operator. Whereas, when subsystem A has a finite length, we show that the middle time behavior of $\log d$ of PRE in RCFTs gradually disappears as the distance between operators or the order number n increases (see figure2(c) and figure 7(c) respectively). Unlike the entanglement entropy, we find that in general, there is a hump during the evolution between the early and late time evolution of the nth PRE (for example, see figure (7)(a)), and for $n = 2$, its peak value can be found as $\Delta S_A^{(2)}(\eta, \bar{\eta}) = \Delta S_A^{(2)}(1/2, 0)$, where $(\eta, \bar{\eta})$ are cross ratios.

On the other hand, for excitation by a linear combination of operators, using Schmidt decomposition, we find that the late time limit of the nth pseudo-Rényi entropy is governed by the formula (65). A prominent property that distinguishes linear combination excitation from single primary operator excitation is that the late limit of PRE under linear combination excitation is not necessarily the same as that of Rényi entropy (see, for example, figure 5(c)). This means that for the case of a single primary operator, the initial information about the positions of the insertion operators is lost in the long-time evolution. In contrast, for the case of linear combinations, the late limit of the pseudo-Rényi entropy still contains the initial information of the operator positions. It would be interesting to explore whether it is possible to recover the initial data by using the late time limit of pseudo-Rényi entropy.

Finally, building on the analysis of the cross ratios, we uncover three kinds of symmetries for the 2nd PRE (47-49), which naturally screen out two kinds of special space configurations of insertion operators—$x_1 = -x_2$ for subsystem $A = [0, \infty)$ and $x_1 = L - x_2$ for subsystem $A = [0, L]$. It can be shown that the trace of $\left(\mathcal{T}_A^{(2)}(t)\right)^2$ is always real in both configurations, and we expect $\text{Tr}\left[\left(\mathcal{T}_A^{(2)}(t)\right)^2\right]$ to be constant positive in the second configuration, which gives us a real 2nd PRE evolution. For the first configuration, although the evolution of PRE under it is not always real, in some theories, the evolution of PRE under the first configuration in $A = [0, \infty)$ shows the same evolutionary pattern as Rényi entropy (see figure 2(a) in the free scalar theory, figure 4(a) in the WZW models, and figure 7(b) in the critical Ising model), i.e., we may have

$$\Delta S_{A=[0,\infty)}^{(n)}(x, -x, t) = \begin{cases} 0, & 0 \le t < |x|, \\ \log d, & t > |x|. \end{cases} \tag{79}$$

It will be an attractive research direction for us in the future to fully clarify the condition

that PRE remains real in the time evolution process and the condition that PRE behaves as Rényi entropy in the first symmetric space configuration. Furthermore, it's also interesting to make a higher-dimensional generalization of our results and dig out the possible corresponding holographic counterpart.

Acknowledgements

A   Several time limits of cross ratios

In this appendix, we will analyze the cross ratios in various limits under two configurations of the subsystem A.

A.1 $A = [0, \infty)$

For the case of $A = [0, \infty)$, the cross ratios in Euclidean signature can be expressed in polar coordinates on Σ_2 as follows

$$
\begin{aligned}
\eta &= \frac{1}{2} - \frac{(r_1 + r_2)\cos\left(\frac{\theta_1 - \theta_2}{2}\right) + i(r_1 - r_2)\sin\left(\frac{\theta_1 - \theta_2}{2}\right)}{4\sqrt{r_1}\sqrt{r_2}}, \\
\bar{\eta} &= \frac{1}{2} - \frac{(r_1 + r_2)\cos\left(\frac{\theta_1 - \theta_2}{2}\right) - i(r_1 - r_2)\sin\left(\frac{\theta_1 - \theta_2}{2}\right)}{4\sqrt{r_1}\sqrt{r_2}},
\end{aligned}
\tag{80}
$$

where $(r_1 \cos\theta_1, r_1 \sin\theta_1) = (x_1, -\tau_1)$, $(r_2 \cos\theta_2, r_2 \sin\theta_2) = (x_2, \tau_2)$, $(0 \leq \theta_j < 2\pi, \ j = 1, 2)$, and

$$
\cos(\theta_1 - \theta_2) = 2\cos^2\left(\frac{\theta_1 - \theta_2}{2}\right) - 1 = 1 - 2\sin^2\left(\frac{\theta_1 - \theta_2}{2}\right) = \frac{x_1 x_2 - \tau_1 \tau_2}{\sqrt{(x_1^2 + \tau_1^2)}\sqrt{(x_2^2 + \tau_2^2)}}.
\tag{81}
$$

Since the two Euclidean times τ_1 and τ_2 after analytic continuation are $\epsilon + it$ and $\epsilon - it$, respectively, we may set $\tau_1 = \tau_2 = \epsilon$ before the analytic continuation. It leads to two ranges of $\theta_1 - \theta_2$ which depend on $x_1 + x_2$: $0 < \theta_1 - \theta_2 < \pi$ when $x_1 + x_2 < 0$; $\pi < \theta_1 - \theta_2 < 2\pi$ when $x_1 + x_2 > 0$. Thus we have the following expressions of $\sin(\cos)\left(\frac{\theta_1 - \theta_2}{2}\right)$ after the analytic continuation

$$
\begin{aligned}
\cos\left(\frac{\theta_1 - \theta_2}{2}\right) &= \left(\frac{1}{2} + \frac{x_1 x_2 - \epsilon^2 - t^2}{2\sqrt{(x_1^2 + (\epsilon + it)^2)}\sqrt{(x_2^2 + (\epsilon - it)^2)}}\right)^{\frac{1}{2}} \text{sgn}[-(x_1 + x_2)], \\
\sin\left(\frac{\theta_1 - \theta_2}{2}\right) &= \left(\frac{1}{2} - \frac{x_1 x_2 - \epsilon^2 - t^2}{2\sqrt{(x_1^2 + (\epsilon + it)^2)}\sqrt{(x_2^2 + (\epsilon - it)^2)}}\right)^{\frac{1}{2}},
\end{aligned}
\tag{82}
$$

where we define

$$\text{sgn}[x] \equiv \begin{cases} 1, & x > 0, \\ -1, & x < 0. \end{cases} \tag{83}$$

Substituting (82) into (80), and let

$$r_1 = \sqrt{x_1^2 + (\epsilon + it)^2}, \quad r_2 = \sqrt{x_2^2 + (\epsilon - it)^2}, \tag{84}$$

we find that the cross ratios can be expressed as

$$\eta(x_1, x_2, t) = \frac{(x_1 + x_2 + 2t) + 2\sqrt{(x_1 + t)(x_2 + t) + \epsilon^2 + i\epsilon(x_1 - x_2)}}{4\sqrt{(x_1 + t)(x_2 + t) + \epsilon^2 + i\epsilon(x_1 - x_2)}},$$

$$\bar{\eta}(x_1, x_2, t) = \frac{(x_1 + x_2 - 2t) + 2\sqrt{(x_1 - t)(x_2 - t) + \epsilon^2 - i\epsilon(x_1 - x_2)}}{4\sqrt{(x_1 - t)(x_2 - t) + \epsilon^2 - i\epsilon(x_1 - x_2)}}. \tag{85}$$

As $x_1 = x_2 = -l < 0$, the above result coincides with that of [35]. According to (85), one can evaluate the early time limit and late time limits for cross ratios

$$\lim_{t \to \infty} (\eta, \bar{\eta}) \simeq \left(1 + \frac{(x_2 - x_1 + 2i\epsilon)^2}{16t^2}, -\frac{(x_2 - x_1 - 2i\epsilon)^2}{16t^2} \right) \simeq (1, 0), \tag{86}$$

$$\lim_{t \to 0} (\eta, \bar{\eta}) \simeq \begin{cases} \left(\frac{1}{2} + \frac{x_1 + x_2}{4\sqrt{x_1 x_2}}, \frac{1}{2} + \frac{x_1 + x_2}{4\sqrt{x_1 x_2}} \right), & x_1 x_2 > 0, \\ \left(\frac{1}{2} + \frac{x_1 + x_2}{4\sqrt{x_1 x_2}}, \frac{1}{2} - \frac{x_1 + x_2}{4\sqrt{x_1 x_2}} \right), & x_1 > 0 > x_2, \\ \left(\frac{1}{2} - \frac{x_1 + x_2}{4\sqrt{x_1 x_2}}, \frac{1}{2} + \frac{x_1 + x_2}{4\sqrt{x_1 x_2}} \right), & x_2 > 0 > x_1. \end{cases} \tag{87}$$

A.2 $A = [0, L]$

For the case of $A = [0, L]$, we can write the Euclidean cross ratios in polar coordinates

$$\eta = \frac{1}{2} - \frac{(r_1 r_4 + r_2 r_3) \cos\left(\frac{\theta_1 - \theta_2 - \theta_3 + \theta_4}{2}\right) + i(r_1 r_4 - r_2 r_3) \sin\left(\frac{\theta_1 - \theta_2 - \theta_3 + \theta_4}{2}\right)}{4\sqrt{r_1}\sqrt{r_2}\sqrt{r_3}\sqrt{r_4}},$$

$$\bar{\eta} = \frac{1}{2} - \frac{(r_1 r_4 + r_2 r_3) \cos\left(\frac{\theta_1 - \theta_2 - \theta_3 + \theta_4}{2}\right) - i(r_1 r_4 - r_2 r_3) \sin\left(\frac{\theta_1 - \theta_2 - \theta_3 + \theta_4}{2}\right)}{4\sqrt{r_1}\sqrt{r_2}\sqrt{r_3}\sqrt{r_4}}, \tag{88}$$

where $(r_1 \cos\theta_1, r_1 \sin\theta_1) = (x_1, -\tau_1)$, $(r_2 \cos\theta_2, r_2 \sin\theta_2) = (x_2, \tau_2)$, $(r_3 \cos\theta_3, r_3 \sin\theta_3) = (x_1 - L, -\tau_1)$, $(r_4 \cos\theta_4, r_4 \sin\theta_4) = (x_2 - L, \tau_2)$ $(0 \le \theta_j < 2\pi,\ j = 1, 2, 3, 4)$, and

$$\cos(\theta_1 - \theta_2) = 2\cos^2\left(\frac{\theta_1 - \theta_2}{2}\right) - 1 = 1 - 2\sin^2\left(\frac{\theta_1 - \theta_2}{2}\right) = \frac{x_1 x_2 - \tau_1 \tau_2}{\sqrt{(x_1^2 + \tau_1^2)}\sqrt{(x_2^2 + \tau_2^2)}},$$

$$\cos(\theta_3 - \theta_4) = 2\cos^2\left(\frac{\theta_3 - \theta_4}{2}\right) - 1 = 1 - 2\sin^2\left(\frac{\theta_3 - \theta_4}{2}\right) = \frac{(x_1 - L)(x_2 - L) - \tau_1 \tau_2}{\sqrt{(x_1 - L)^2 + \tau_1^2}\sqrt{(x_2 - L)^2 + \tau_2^2}}. \tag{89}$$

Similar to the arguments in Appendix A.1 , we obtain the expressions of $\sin(\cos)\left(\frac{\theta_1 - \theta_2}{2}\right)$ and $\sin(\cos)\left(\frac{\theta_3 - \theta_4}{2}\right)$ after the analytic continuation as follows

$$\cos\left(\frac{\theta_1 - \theta_2}{2}\right) = \left(\frac{1}{2} + \frac{x_1 x_2 - \epsilon^2 - t^2}{2\sqrt{(x_1^2 + (\epsilon + it)^2)}\sqrt{(x_2^2 + (\epsilon - it)^2)}}\right)^{\frac{1}{2}} \text{sgn}[-(x_1 + x_2)],$$

$$\sin\left(\frac{\theta_1 - \theta_2}{2}\right) = \left(\frac{1}{2} - \frac{x_1 x_2 - \epsilon^2 - t^2}{2\sqrt{(x_1^2 + (\epsilon + it)^2)}\sqrt{(x_2^2 + (\epsilon - it)^2)}}\right)^{\frac{1}{2}},$$

$$\cos\left(\frac{\theta_3 - \theta_4}{2}\right) = \left(\frac{1}{2} + \frac{(x_1 - L)(x_2 - L) - \epsilon^2 - t^2}{2\sqrt{(x_1 - L)^2 + (\epsilon + it)^2}\sqrt{(x_2 - L)^2 + (\epsilon - it)^2}}\right)^{\frac{1}{2}} \text{sgn}[2L - (x_1 + x_2)],$$

$$\sin\left(\frac{\theta_3 - \theta_4}{2}\right) = \left(\frac{1}{2} - \frac{(x_1 - L)(x_2 - L) - \epsilon^2 - t^2}{2\sqrt{(x_1 - L)^2 + (\epsilon + it)^2}\sqrt{(x_2 - L)^2 + (\epsilon - it)^2}}\right)^{\frac{1}{2}}, \tag{90}$$

where $\text{sgn}[x]$ is the sign function (83) that we define. Substituting (90) into (88), and let

$$r_1 = \sqrt{x_1^2 + (\epsilon + it)^2}, \qquad r_2 = \sqrt{x_2^2 + (\epsilon - it)^2},$$
$$r_3 = \sqrt{(x_1 - L)^2 + (\epsilon + it)^2}, \quad r_4 = \sqrt{(x_2 - L)^2 + (\epsilon - it)^2}, \tag{91}$$

we find that the cross ratios can be expressed as

$$\eta(x_1, x_2, t) = \frac{(x_1 + x_2 + 2t)L\left[(L - x_1 - t)(L - x_2 - t) + \epsilon^2 + i\epsilon(x_1 - x_2)\right]^{-\frac{1}{2}}}{4\sqrt{(x_1 + t)(x_2 + t) + \epsilon^2 + i\epsilon(x_1 - x_2)}}$$
$$+ \frac{1}{2}\left(1 - \sqrt{\frac{(x_1 + t)(x_2 + t) + \epsilon^2 + i\epsilon(x_1 - x_2)}{(L - x_1 - t)(L - x_2 - t) + \epsilon^2 + i\epsilon(x_1 - x_2)}}\right),$$

$$\bar{\eta}(x_1, x_2, t) = \frac{(x_1 + x_2 - 2t)L\left[(L - x_1 + t)(L - x_2 + t) + \epsilon^2 - i\epsilon(x_1 - x_2)\right]^{-\frac{1}{2}}}{4\sqrt{(x_1 - t)(x_2 - t) + \epsilon^2 - i\epsilon(x_1 - x_2)}}$$
$$+ \frac{1}{2}\left(1 - \sqrt{\frac{(x_1 - t)(x_2 - t) + \epsilon^2 - i\epsilon(x_1 - x_2)}{(L - x_1 + t)(L - x_2 + t) + \epsilon^2 - i\epsilon(x_1 - x_2)}}\right). \tag{92}$$

As a self-consistent test, it can be found that (92) degenerates to (85) as $L \to \infty$.

B Derivation of Eq.(65)

Let us first define a series of normalized excited states with the help of $\mathcal{O}_p$

$$|\mathcal{O}_p(x)\rangle := \frac{1}{\sqrt{\langle \mathcal{O}_p^\dagger(x, \epsilon)\mathcal{O}_p(x, -\epsilon)\rangle}}\mathcal{O}_p(x, -\epsilon)|\Omega\rangle,$$

$$\left(\langle \mathcal{O}_{p'}(x')|\mathcal{O}_p(x)\rangle = \frac{\delta_{pp'} \cdot \langle \mathcal{O}_p^\dagger(x', \epsilon)\mathcal{O}_p(x, -\epsilon)\rangle}{\sqrt{\langle \mathcal{O}_p^\dagger(x, \epsilon)\mathcal{O}_p(x, -\epsilon)\rangle\langle \mathcal{O}_p^\dagger(x', \epsilon)\mathcal{O}_p(x', -\epsilon)\rangle}}\right). \tag{93}$$

$|\psi\rangle$ and $|\tilde{\psi}\rangle$ can be written as two superposition states of $|\mathcal{O}_p\rangle$

$$|\psi\rangle = \sum_p \sqrt{\lambda_p}|\mathcal{O}_p(x)\rangle, \quad |\tilde{\psi}\rangle = \sum_p \sqrt{\tilde{\lambda}_p}|\mathcal{O}_p(\tilde{x})\rangle, \tag{94}$$

where

$$\lambda_p = \frac{(C_p)^2\langle\mathcal{O}_p^\dagger(x,\epsilon)\mathcal{O}_p(x,-\epsilon)\rangle}{\sum_{p'}|C_{p'}|^2\langle\mathcal{O}_{p'}^\dagger(x,\epsilon)\mathcal{O}_{p'}(x,-\epsilon)\rangle}, \quad \sum_p|\lambda_p| = 1,$$

$$\tilde{\lambda}_p = \frac{(\tilde{C}_p)^2\langle\mathcal{O}_p^\dagger(\tilde{x},\epsilon)\mathcal{O}_p(\tilde{x},-\epsilon)\rangle}{\sum_{p'}|\tilde{C}_{p'}|^2\langle\mathcal{O}_{p'}^\dagger(\tilde{x},\epsilon)\mathcal{O}_{p'}(\tilde{x},-\epsilon)\rangle}, \quad \sum_p|\tilde{\lambda}_p| = 1. \tag{95}$$

Generally speaking, $|\mathcal{O}_p\rangle$ is an entangled state living in the sub-Verma module $H_p \bigotimes H_{\bar{p}}$. It can be written in the following form by Schmidt decomposition

$$|\mathcal{O}_p(x)\rangle = \sum_i a_i^p(x)|p_i(x)\rangle \otimes |(\bar{p}_i(x)\rangle, \tag{96}$$

where $\{|p_i(x)\rangle\}$ and $\{|\bar{p}_i(x)\rangle\}$ parameterized by x are two orthonormal basises of H_p and $H_{\bar{p}}$ repectively, and $a_i^p(x)$ are real coefficients. In these basisies the nth Rényi entropy of $|\mathcal{O}_p(x)\rangle$ reads

$$S^{(n)}[\mathcal{O}_p(x)] = \frac{1}{1-n}\log\left\{\text{Tr}_{(\oplus_p H_p)}\left[\left(\text{Tr}_{(\oplus_p H_{\bar{p}})}|\mathcal{O}_p(x)\rangle\langle\mathcal{O}_p(x)|\right)^n\right]\right\} = \frac{1}{1-n}\log\sum_i\left(a_i^p(x)\right)^{2n}, \tag{97}$$

meanwhile, the transition matrix becomes

$$\mathcal{T}^{\psi|\tilde{\psi}} = \frac{1}{\sum_p\sqrt{\lambda_p}\sqrt{\tilde{\lambda}_p^*}\langle\mathcal{O}_p(\tilde{x})|\mathcal{O}_p(x)\rangle}\sum_{p,p'}\sqrt{\lambda_p}\sqrt{\tilde{\lambda}_{p'}^*}\sum_{i,j}a_i^p(x)a_j^{p'}(\tilde{x})|p_i(x)\rangle|\bar{p}_i(x)\rangle\langle p_j'(\tilde{x})|\langle\bar{p}_j'(\tilde{x})|. \tag{98}$$

The reduce transition matrix is obtained by tracing out the anti-holomorphic part,

$$\mathcal{T}_H^{\psi|\tilde{\psi}} = \text{Tr}_{\oplus_{\bar{p}} H_{\bar{p}}}\mathcal{T}^{\psi|\tilde{\psi}}$$

$$= \sum_p\sum_{i,j,k}\frac{\sqrt{\lambda_p}\sqrt{\tilde{\lambda}_p^*}a_i^p(x)a_j^p(\tilde{x})\langle\bar{p}_j(\tilde{x})|\bar{p}_i(x)\rangle\langle p_j(\tilde{x})|p_k(x)\rangle}{\sum_{p''}\sqrt{\lambda_{p''}}\sqrt{\tilde{\lambda}_{p''}^*}\langle\mathcal{O}_{p''}(\tilde{x})|\mathcal{O}_{p''}(x)\rangle} \cdot |p_i(x)\rangle\langle p_k(x)|, \tag{99}$$

which in general is off-diagonal. We can compute the trace of $(\mathcal{T}_H^{\psi|\tilde{\psi}})^n$,

$$\text{Tr}\left[(\mathcal{T}_H^{\psi|\tilde{\psi}})^n\right]$$

$$= \sum_p\frac{\left(\sqrt{\lambda_p}\sqrt{\tilde{\lambda}_p^*}\right)^n}{\left(\sum_{p''}\sqrt{\lambda_{p''}}\sqrt{\tilde{\lambda}_{p''}^*}\langle\mathcal{O}_{p''}(\tilde{x})|\mathcal{O}_{p''}(x)\rangle\right)^n}$$

$$\times \sum_{\{i\},\{j\}}a_{i_1}^p(x)a_{j_1}^p(\tilde{x})\langle\bar{p}_{j_1}(\tilde{x})|\bar{p}_{i_1}(x)\rangle\langle p_{j_1}(\tilde{x})|p_{i_2}(x)\rangle...a_{i_n}^p(x)a_{j_n}^p(\tilde{x})\langle\bar{p}_{j_n}(\tilde{x})|\bar{p}_{i_n}(x)\rangle\langle p_{j_n}(\tilde{x})|p_{i_1}(x)\rangle. \tag{100}$$

To further reduce (100), let us turn to consider a more straightforward case that

$$|\phi(t)\rangle = \mathrm{e}^{-iHt}|\mathcal{O}_p(x)\rangle, \quad |\tilde{\phi}(t)\rangle = \mathrm{e}^{-iHt}|\mathcal{O}_p(\tilde{x})\rangle. \tag{101}$$

According to the analysis in section 4, we know that the late time limit of $\Delta S^{(n)}\big[\mathcal{T}_A^{\phi|\tilde{\phi}}(t)\big]$ is equal to $\lim_{t\to\infty}\Delta S^{(n)}\big[\mathrm{Tr}_{A^c}|\phi(t)\rangle\langle\phi(t)|\big]$, and the latter we already know is equal to (97) [42]. On the other hand, following the logic in [42], it's natural to expect that

$$
\begin{aligned}
&\lim_{t\to\infty} \Delta S_A^{(n)}\big[\mathcal{T}^{\phi|\tilde{\phi}}(t)\big]\\
=&\frac{1}{1-n}\log \mathrm{Tr}_{\oplus_p H_p}\Big[\big(\mathcal{T}_H^{\phi(0)|\tilde{\phi}(0)}\big)^n\Big]\\
=&\frac{1}{1-n}\log\Big[\langle\mathcal{O}_p(\tilde{x})|\mathcal{O}_p(x)\rangle^{-n}\\
&\times \sum_{\{i\},\{j\}} \alpha_{i_1}^p(x)\alpha_{j_1}^p(\tilde{x})\langle\bar{p}_{j_1}(\tilde{x})|\bar{p}_{i_1}(x)\rangle\langle p_{j_1}(\tilde{x})|p_{i_2}(x)\rangle...\alpha_{i_n}^p(x)\alpha_{j_n}^p(\tilde{x})\langle\bar{p}_{j_n}(\tilde{x})|\bar{p}_{i_n}(x)\rangle\langle p_{j_n}(\tilde{x})|p_{i_1}(x)\rangle\Big]
\end{aligned}
\tag{102}
$$

Comparing Eq.(97) with Eq.(102), we obtain the equality

$$
\begin{aligned}
&\sum_{\{i\},\{j\}} \alpha_{i_1}^p(x)\alpha_{j_1}^p(\tilde{x})\langle\bar{p}_{j_1}(\tilde{x})|\bar{p}_{i_1}(x)\rangle\langle p_{j_1}(\tilde{x})|p_{i_2}(x)\rangle...\alpha_{i_n}^p(x)\alpha_{j_n}^p(\tilde{x})\langle\bar{p}_{j_n}(\tilde{x})|\bar{p}_{i_n}(x)\rangle\langle p_{j_n}(\tilde{x})|p_{i_1}(x)\rangle\\
=&\langle\mathcal{O}_p(\tilde{x})|\mathcal{O}_p(x)\rangle^n \sum_i \big(a_i^p(x)\big)^{2n}
\end{aligned}
\tag{103}
$$

Substituting Eq.(103) into Eq.(100) and taking some algebra, we finally obtain

$$\frac{1}{1-n}\log \mathrm{Tr}\Big[(\mathcal{T}_H^{\psi|\tilde{\psi}})^n\Big] = \frac{1}{1-n}\log\left[\sum_p \left(\frac{C_p\tilde{C}_p^*\langle\mathcal{O}_p^\dagger(\tilde{w},\bar{\tilde{w}})\mathcal{O}_p(w,\bar{w})\rangle}{\sum_{p'}C_{p'}\tilde{C}_{p'}^*\langle\mathcal{O}_{p'}^\dagger(\tilde{w},\bar{\tilde{w}})\mathcal{O}_{p'}(w,\bar{w})\rangle}\right)^n \mathrm{e}^{(1-n)S^{(n)}[\mathcal{O}_p]}\right], \tag{104}$$

which, in the light of the logic in [42], just corresponds to the late time limit of nth pseudo-Rényi entropy of A. Let $\{\tilde{C}_p\} = \{C_p\} = 1$ and $\tilde{x} = x$, it can be readily found that (104) is reduced to the Eq.(2.26) in [42].

References

[1] G. Vidal, J. I. Latorre, E. Rico and A. Kitaev, Entanglement in quantum critical phenomena, Phys. Rev. Lett. **90** (2003) 227902, [quant-ph/0211074].

[2] A. Kitaev and J. Preskill, Topological entanglement entropy, Phys. Rev. Lett. **96** (2006) 110404, [hep-th/0510092].

[3] M. Levin and X.-G. Wen, Detecting topological order in a ground state wave function, Phys. Rev. Lett. **96** (Mar, 2006) 110405.

[4] L. Bombelli, R. K. Koul, J. Lee and R. D. Sorkin,
A Quantum Source of Entropy for Black Holes, Phys. Rev. D **34** (1986) 373–383.

[5] M. Srednicki, Entropy and area, Phys. Rev. Lett. **71** (1993) 666–669, [hep-th/9303048].

[6] P. Calabrese and J. L. Cardy, Entanglement entropy and quantum field theory, J. Stat. Mech. **0406** (2004) P06002, [hep-th/0405152].

[7] H. Casini and M. Huerta, Entanglement entropy in free quantum field theory, J. Phys. A **42** (2009) 504007, [0905.2562].

[8] T. Nishioka, Entanglement entropy: holography and renormalization group, Rev. Mod. Phys. **90** (2018) 035007, [1801.10352].

[9] S. Ryu and T. Takayanagi,
Holographic derivation of entanglement entropy from AdS/CFT, Phys. Rev. Lett. **96** (2006) 181602, [hep-th/0603001].

[10] V. E. Hubeny, M. Rangamani and T. Takayanagi,
A Covariant holographic entanglement entropy proposal, JHEP **07** (2007) 062, [0705.0016].

[11] B. Swingle, Entanglement Renormalization and Holography, Phys. Rev. D **86** (2012) 065007, [0905.1317].

[12] J. Maldacena and L. Susskind, Cool horizons for entangled black holes, Fortsch. Phys. **61** (2013) 781–811, [1306.0533].

[13] A. Almheiri, T. Hartman, J. Maldacena, E. Shaghoulian and A. Tajdini,
The entropy of Hawking radiation, Rev. Mod. Phys. **93** (2021) 035002, [2006.06872].

[14] N. Engelhardt and A. C. Wall,
Quantum Extremal Surfaces: Holographic Entanglement Entropy beyond the Classical Regime, JHEP **01** (2015) 073, [1408.3203].

[15] J. M. Maldacena, The Large N limit of superconformal field theories and supergravity, Adv. Theor. Math. Phys. **2** (1998) 231–252, [hep-th/9711200].

[16] S. S. Gubser, I. R. Klebanov and A. M. Polyakov,
Gauge theory correlators from noncritical string theory, Phys. Lett. B **428** (1998) 105–114, [hep-th/9802109].

[17] E. Witten, Anti-de Sitter space and holography, Adv. Theor. Math. Phys. **2** (1998) 253–291, [hep-th/9802150].

[18] S. W. Hawking, Breakdown of Predictability in Gravitational Collapse, Phys. Rev. D **14** (1976) 2460–2473.

[19] S. D. Mathur, The Information paradox: A Pedagogical introduction, Class. Quant. Grav. **26** (2009) 224001, [0909.1038].

[20] Y. Nakata, T. Takayanagi, Y. Taki, K. Tamaoka and Z. Wei, New holographic generalization of entanglement entropy, Phys. Rev. D **103** (2021) 026005, [2005.13801].

[21] I. Akal, T. Kawamoto, S.-M. Ruan, T. Takayanagi and Z. Wei, On the Page curve under final state projection, 2112.08433.

[22] D. N. Page, Average entropy of a subsystem, Phys. Rev. Lett. **71** (1993) 1291–1294, [gr-qc/9305007].

[23] G. T. Horowitz and J. M. Maldacena, The Black hole final state, JHEP **02** (2004) 008, [hep-th/0310281].

[24] I. Akal, Y. Kusuki, N. Shiba, T. Takayanagi and Z. Wei, Entanglement Entropy in a Holographic Moving Mirror and the Page Curve, Phys. Rev. Lett. **126** (2021) 061604, [2011.12005].

[25] A. Mollabashi, N. Shiba, T. Takayanagi, K. Tamaoka and Z. Wei, Pseudo Entropy in Free Quantum Field Theories, Phys. Rev. Lett. **126** (2021) 081601, [2011.09648].

[26] G. Camilo and A. Prudenziati, Twist operators and pseudo entropies in two-dimensional momentum space, 2101.02093.

[27] A. Mollabashi, N. Shiba, T. Takayanagi, K. Tamaoka and Z. Wei, Aspects of pseudoentropy in field theories, Phys. Rev. Res. **3** (2021) 033254, [2106.03118].

[28] T. Nishioka, T. Takayanagi and Y. Taki, Topological pseudo entropy, JHEP **09** (2021) 015, [2107.01797].

[29] K. Goto, M. Nozaki and K. Tamaoka, Subregion spectrum form factor via pseudoentropy, Phys. Rev. D **104** (2021) L121902, [2109.00372].

[30] M. Miyaji, Island for gravitationally prepared state and pseudo entanglement wedge, JHEP **12** (2021) 013, [2109.03830].

[31] J. Mukherjee, Pseudo Entropy in $U(1)$ gauge theory, 2205.08179.

[32] M. Nozaki, T. Numasawa and T. Takayanagi,
Quantum Entanglement of Local Operators in Conformal Field Theories, Phys. Rev.
Lett. **112** (2014) 111602, [1401.0539].

[33] S. He, T. Numasawa, T. Takayanagi and K. Watanabe,
Quantum dimension as entanglement entropy in two dimensional conformal field theories,
Phys. Rev. D **90** (2014) 041701, [1403.0702].

[34] P. Caputa and A. Veliz-Osorio, Entanglement constant for conformal families, Phys. Rev.
D **92** (2015) 065010, [1507.00582].

[35] B. Chen, W.-Z. Guo, S. He and J.-q. Wu,
Entanglement Entropy for Descendent Local Operators in 2D CFTs, JHEP **10** (2015)
173, [1507.01157].

[36] S. He, Conformal bootstrap to Rényi entropy in 2D Liouville and super-Liouville CFTs,
Phys. Rev. D **99** (2019) 026005, [1711.00624].

[37] P. Caputa, M. Nozaki and T. Takayanagi,
Entanglement of local operators in large-N conformal field theories, PTEP **2014** (2014)
093B06, [1405.5946].

[38] P. Caputa, T. Numasawa and A. Veliz-Osorio,
Out-of-time-ordered correlators and purity in rational conformal field theories, PTEP
2016 (2016) 113B06, [1602.06542].

[39] W.-Z. Guo and S. He,
Rényi entropy of locally excited states with thermal and boundary effect in 2D CFTs,
JHEP **04** (2015) 099, [1501.00757].

[40] L. Apolo, S. He, W. Song, J. Xu and J. Zheng,
Entanglement and chaos in warped conformal field theories, JHEP **04** (2019) 009,
[1812.10456].

[41] P. Caputa, J. Simón, A. Štikonas and T. Takayanagi,
Quantum Entanglement of Localized Excited States at Finite Temperature, JHEP **01**
(2015) 102, [1410.2287].

[42] W.-Z. Guo, S. He and Z.-X. Luo,
Entanglement entropy in (1+1)D CFTs with multiple local excitations, JHEP **05** (2018)
154, [1802.08815].

[43] M. Nozaki, T. Numasawa and T. Takayanagi,
Holographic Local Quenches and Entanglement Density, JHEP **05** (2013) 080,
[1302.5703].

[44] D. S. Ageev, Holographic local quench at finite chemical potential, Eur. Phys. J. Plus
136 (2021) 1178.

[45] N. Zenoni, A falling magnetic monopole as a local quench, PoS **EPS-HEP2021** (2022)
722.

[46] T. Kawamoto, T. Mori, Y.-k. Suzuki, T. Takayanagi and T. Ugajin,
Holographic Local Operator Quenches in BCFTs, 2203.03851.

[47] P. Calabrese and J. L. Cardy,
Evolution of entanglement entropy in one-dimensional systems, J. Stat. Mech. **0504**
(2005) P04010, [cond-mat/0503393].

[48] C. T. Asplund, A. Bernamonti, F. Galli and T. Hartman,
Entanglement Scrambling in 2d Conformal Field Theory, JHEP **09** (2015) 110,
[1506.03772].

[49] M. Nozaki, Notes on Quantum Entanglement of Local Operators, JHEP **10** (2014) 147,
[1405.5875].

[50] A. A. Belavin, A. M. Polyakov and A. B. Zamolodchikov,
Infinite Conformal Symmetry in Two-Dimensional Quantum Field Theory, Nucl. Phys.
B **241** (1984) 333–380.

[51] G. W. Moore and N. Seiberg,
Polynomial Equations for Rational Conformal Field Theories, Phys. Lett. B **212** (1988)
451–460.

[52] G. W. Moore and N. Seiberg, Naturality in Conformal Field Theory, Nucl. Phys. B **313**
(1989) 16–40.

[53] V. Fateev and S. Ribault, The Large central charge limit of conformal blocks, JHEP **02**
(2012) 001, [1109.6764].

[54] A. B. Zamolodchikov,
CONFORMAL SYMMETRY IN TWO-DIMENSIONS: AN EXPLICIT RECURRENCE FORMULA
Commun. Math. Phys. **96** (1984) 419–422.

[55] P. Di Francesco, H. Saleur and J. B. Zuber,
Critical Ising Correlation Functions in the Plane and on the Torus, Nucl. Phys. B **290**
(1987) 527.

[56] V. S. Dotsenko and V. A. Fateev,
Conformal Algebra and Multipoint Correlation Functions in Two-Dimensional Statistical Models,
Nucl. Phys. B **240** (1984) 312.

[57] V. S. Dotsenko and V. A. Fateev,
Four Point Correlation Functions and the Operator Algebra in the Two-Dimensional Conformal Inv
Nucl. Phys. B **251** (1985) 691–734.

[58] V. G. Knizhnik and A. B. Zamolodchikov,
Current Algebra and Wess-Zumino Model in Two-Dimensions, Nucl. Phys. B **247** (1984)
83–103.

[59] A. Luther and I. Peschel,
Calculation of critical exponents in two-dimensions from quantum field theory in one-dimension,
Phys. Rev. B **12** (1975) 3908–3917.